

## Functional assessment of SLC4A11, an integral membrane protein mutated in corneal dystrophies

[Sampath K. Loganathan](#),<sup>1</sup> [Hans-Peter Schneider](#),<sup>2</sup> [Patricio E. Morgan](#),<sup>3</sup> [Joachim W. Deitmer](#),<sup>2</sup> and [Joseph R. Casey](#)<sup>✉1</sup>

<sup>1</sup>Department of Biochemistry, Membrane Protein Disease Research Group, University of Alberta, Edmonton, Alberta, Canada;

<sup>2</sup>Abteilung für Allgemeine Zoologie, Fachbereich Biologie, Technische Universität Kaiserslautern, Kaiserslautern, Germany; and

<sup>3</sup>Centro de Investigaciones Cardiovasculares, Facultad de Ciencias Médicas, Universidad Nacional de La Plata, La Plata, Buenos Aires, Argentina

<sup>✉</sup>Corresponding author.

Address for reprint requests and other correspondence: J. R. Casey, Dept. of Biochemistry, Univ. of Alberta, Edmonton, AB, Canada T6G 2H7 (e-mail: [joe.casey@ualberta.ca](mailto:joe.casey@ualberta.ca)).

Received 2016 Mar 22; Accepted 2016 Aug 17.

Copyright © 2016 the American Physiological Society

### Abstract

[Go to:](#)

SLC4A11, a member of the SLC4 family of bicarbonate transporters, is a widely expressed integral membrane protein, abundant in kidney and cornea. Mutations of SLC4A11 cause some cases of the blinding corneal dystrophies, congenital hereditary endothelial dystrophy, and Fuchs endothelial corneal dystrophy. These diseases are marked by fluid accumulation in the corneal stroma, secondary to defective fluid reabsorption by the corneal endothelium. The role of SLC4A11 in these corneal dystrophies is not firmly established, as SLC4A11 function remains unclear. To clarify the normal function(s) of SLC4A11, we characterized the protein following expression in the simple, low-background expression system *Xenopus laevis* oocytes. Since plant and fungal SLC4A11 orthologs transport borate, we measured cell swelling associated with accumulation of solute borate. The plant water/borate transporter NIP5;1 manifested borate transport, whereas human SLC4A11 did not. SLC4A11 supported osmotically driven water accumulation that was electroneutral and Na<sup>+</sup> independent. Studies in oocytes and HEK293 cells could not detect Na<sup>+</sup>-coupled HCO<sub>3</sub><sup>-</sup> transport or Cl<sup>-</sup>/HCO<sub>3</sub><sup>-</sup> exchange by SLC4A11. SLC4A11 mediated electroneutral NH<sub>3</sub> transport in oocytes. Voltage-dependent OH<sup>-</sup> or H<sup>+</sup> movement was not measurable in SLC4A11-expressing oocytes, but SLC4A11-expressing HEK293 cells manifested low-level cytosolic acidification at baseline. In mammalian cells, but not oocytes, OH<sup>-</sup>/H<sup>+</sup> conductance may arise when SLC4A11 activates another protein or itself is activated by another protein. These data argue against a role of human SLC4A11 in bicarbonate or borate transport. This work provides additional support for water and ammonia transport by SLC4A11. When expressed in oocytes, SLC4A11 transported NH<sub>3</sub>, not NH<sub>3</sub>/H<sup>+</sup>.

**Keywords:** ammonia, corneal dystrophy, endothelial cell, SLC4A11, water flux

MUTATIONS OF SLC4A11 underlie blinding genetic corneal dystrophies. SLC4A11, a member of the SLC4 family of plasma membrane bicarbonate transport proteins (4), is widely expressed in human tissues, but especially highly in cornea, kidney, and choroid plexus (10, 44). The central cornea layer, stroma, has a high concentration of dissolved proteoglycans, which drive osmotic fluid accumulation from the anterior aqueous humor through the endothelial cell layer. Corneal endothelium actively counters the fluid flow in a process known as the endothelial “pump” (7). Failure of components of the endothelial pump gives rise to corneal stromal edema, which can profoundly impair vision (21).

SLC4A11 mutations lead to some cases of the rare, recessive disease congenital hereditary endothelial dystrophy (CHED) (33, 46). Harboyan syndrome (HS), marked by early endothelial dystrophy and

sensorineuronal deafness, is also caused by SLC4A11 mutations (12). More recent analysis, however, suggests that individuals with CHED also develop hearing deficits, suggesting that CHED and HS are not distinct (37). Although genetically heterogeneous, SLC4A11 mutations can also cause common [4% lifetime disease burden (31a)] late-onset dominantly inherited Fuchs endothelial corneal dystrophy (FECD) (2, 47).

The role of SLC4A11 in corneal dystrophy pathogenesis is supported by studies of *slc4a11*-null mice. Three independent mouse lines have undergone *slc4a11* disruption (13, 27, 44), all of which manifested corneal edema, indicating that loss of SLC4A11 function can underlie corneal dystrophies. A urinary concentrating defect was present in one mouse line (13), but this deficit has not been reported in individuals with corneal dystrophies.

Understanding the normal function of SLC4A11 is prerequisite to establishing the protein's dysfunction in corneal dystrophies and in developing therapies to compensate for its loss. SLC4A11 resides in the basolateral membrane of corneal endothelial cells, facing the corneal stroma (44). About 60 point mutants of SLC4A11 have been reported to date (1, 3, 12, 14, 18, 20, 22, 23, 34, 35, 38, 40, 46, 47). Most characterized SLC4A11 mutant proteins display the intracellular retention phenotype characteristic of misfolded membrane proteins. Loss of cell surface SLC4A11 thus explains the disease, as also observed in the mouse deletion strains.

The normal function(s) of SLC4A11, however, remains unclear. While the SLC4 proteins are best known as bicarbonate transporters (4), plant and fungal SLC4A11 orthologs are borate transporters (17, 29). Since the established biological role of borate is to stabilize vicinal diols in cell walls (31), borate transport does not have an obvious role in human physiology. One study found that human SLC4A11 functions in borate transport (32), which subsequently could not be substantiated for bovine or human SLC4A11 (16, 30). Subsequently, human SLC4A11 was found to facilitate Na<sup>+</sup>-dependent (30) or independent (19) H<sup>+</sup> or OH<sup>-</sup> transport. Both mammalian cells and *Xenopus laevis* oocytes expressing human SLC4A11 show increased rates of cell swelling in response to hypo-osmotic challenge, consistent with SLC4A11 forming a water-permeable pore (44). The water channel-like activity of SLC4A11 led to the idea that SLC4A11, like aquaporin proteins, might also be permeable to ammonia (50). Subsequent experiments revealed human SLC4A11 as a NH<sub>3</sub>-H<sup>+</sup> cotransporter when expressed in mammalian cells (50).

To clarify the functions of human SLC4A11, we decided to study the protein by using the *X. laevis* oocyte expression system, which previously had been used only to examine SLC4A11 water permeation (44). Oocytes provide a background with very low endogenous plasma membrane transport or channel activity. Moreover, oocytes lack mammalian proteins that might alter SLC4A11 function. Together, oocytes provide an independent, low-background environment in which to study all reported SLC4A11 functions and to establish the electrical activity associated with these processes. In this study, we examined human SLC4A11 bicarbonate, borate, H<sup>+</sup>/OH<sup>-</sup>, and ammonia transport, using oocytes, complemented in some cases by experiments in transfected HEK293 cells.

## MATERIALS AND METHODS

[Go to:](#)

**Materials.** Oligonucleotides were from Integrated DNA Technologies (Coralville, IA). Q5 mutagenesis kit was from New England Biolabs (Ipswich, MA). Dulbecco's modified Eagle's medium (DMEM), fetal bovine serum, calf serum, penicillin-streptomycin-glutamine, and BCECF-AM were from Life Technologies (Carlsbad, CA). DNA Gel Extraction Kit was from Froggabio (Ontario, Canada). HiSpeed Plus Plasmid Purification Kit was from Qiagen (Mississauga, Canada). Cell culture dishes were from Sarstedt (Montreal, Canada). Complete protease inhibitor tablets were from Roche Applied Science (Indianapolis, IN). BCA Protein Assay Kit was from Pierce (Rockford, IL). Glass coverslips were from Thermo Fisher Scientific (Ottawa, Canada). Nigericin, ethyl-isopropyl amiloride, and poly-L-lysine were from Sigma-Aldrich (Oakville, Canada). Immobilon-P PVDF membranes and Luminata Crescendo reagent were from Millipore (Billerica, MA). Monoclonal antibody against hemagglutinin (HA) (clone 16B12) was from Covance (Princeton, NJ). Horseradish peroxidase-conjugated sheep antimouse IgG was from GE Healthcare Bio-Sciences (Piscataway, NJ). mMessage mMachine in vitro T7 RNA polymerase kit was from Ambion (Austin, TX). Hydrogen ionophore I-cocktail A was from Fluka (Buchs, Switzerland).

**DNA constructs.** N-terminal hemagglutinin epitope tagged splicing variant 2 of human SLC4A11 encoding an 891 amino acid protein (NCBI Reference Sequence: [NG\\_017072.1](#)) in eukaryotic expression construct (pSKL1) was reported earlier (25). N-terminal HA-tagged AQP1 and NIP5;1 in oocyte expression vector pGEMHE were reported earlier (44). SLC4A11 cDNA corresponding to the last 856 amino acids (which are common for all 3 variants) (Darpan Malhotra, unpublished observations) with N-terminal HA-tag was cloned from pGEMHE-SLC4A11 (pGV4) construct that was reported earlier (44). Using Q5 mutagenesis kit, primers 5'-TCGCAGAATGGATACTTCG-3' and 5'-TCCTGCGTAGTCAGGTAC-3' and pGV4 as template, the new construct (pAB5) corresponding to the last 856 amino acids of SLC4A11 with HA-epitope tag was cloned into pGEMHE vector for oocyte expression.

**X. laevis oocyte isolation, maintenance, and expression.** Oocytes were isolated from adult female *X. laevis*, which were housed in an established frog colony and fed regular frog brittle twice weekly. Preparation of oocytes has been described in detail previously (5, 6). All animal procedures conformed with and were performed under approved University of Alberta and Technical University Kaiserslautern protocols.

Oocytes were singularized by collagenase (Worthington, Lakewood, NJ) treatment in Ca<sup>2+</sup>-free oocyte Ringer's solution (82.5 mM NaCl, 2.5 mM KCl, 1 mM MgCl<sub>2</sub>, 1 mM Na<sub>2</sub>HPO<sub>4</sub>, and 5 mM HEPES, pH 7.8) at 28°C for 1.5 h. After digestion, healthy oocytes at stage VI were manually selected on the basis of size and uniformity of color and incubated at 18°C in Ringer's solution, supplemented with 0.1 mg/ml penicillin and 0.05 mg/ml gentamicin sulfate.

Plasmid cDNA was linearized with *NheI* and transcribed with mMessage mMachine in vitro T7 RNA polymerase kit to produce capped RNA transcripts. cRNA was purified and stored at -80°C in diethylpyrocarbonate-treated water. Oocytes at stage V or VI were injected with 4 ng of SLC4A11 cRNA, 1 ng of AQP1 cRNA, or 25 ng of NIP5;1 cRNA by using glass micropipettes and a microinjection device (Nanoliter 2000, World Precision Instruments, Berlin, Germany). Noninjected or water-injected native oocytes were used as a control.

**Measurements of water flux and borate transport.** Oocytes were preincubated with fivefold diluted ND96 solution (96 mM NaCl, 2 mM KCl, 1.8 mM CaCl<sub>2</sub>, 1 mM MgCl<sub>2</sub>, 10.0 mM HEPES, pH 7.4) adjusted to 220 mosmol/kg with mannitol (isotonic solution) for 10 min at room temperature; oocytes were perfused with fivefold diluted ND96 solution (44 mosmol/kg) (hypotonic solution), and the time course of osmotic volume increase was monitored by video microscopy, with images collected every 15 s. Solution osmolarity was assessed with an Advanced Instruments 3D3 osmometer. Image-Pro Plus software (Media Cybernetics, Silver Spring, MD) was used to measure the mean diameter of each oocyte image and then to calculate its volume. Oocyte volumes, plotted as a function of time following exposure to hypotonic buffer, were fitted with a model-independent second-order polynomial, and the initial rates of swelling [d(Vol/Vol<sub>0</sub>)/dt] were calculated from the linear component of the fit. For sodium-free osmotic water flux experiments, NaCl was replaced by choline chloride, and the experiments were performed as described above. For borate transport assays, oocytes were preincubated as described above and then perfused with a ND96 solution diluted fivefold and adjusted to 220 mosmol with boric acid (41). All the solutions were adjusted to pH of 7.4.

**Intracellular pH and membrane current recordings in X. laevis oocytes.** Intracellular pH and membrane potential were measured with double-barreled microelectrodes, which have been described previously (11). Electrodes were calibrated with bicarbonate-free oocyte Ringer's solution with a pH of 7.0 and 7.4. The recording arrangement was described previously (11, 28). Central and reference barrels of the electrodes were connected with chloride-treated silver wires to the head stages of an Axoclamp 2B amplifier (Axon Instruments). Electrodes were able to detect pH changes in saline solution with higher temporal resolution than the fastest reaction expected to occur in the cytoplasm of the oocyte. As described previously, optimal intracellular oocyte pH measurements were detected when the electrode was located near the intracellular surface of the plasma membrane, which was achieved by carefully rotating the oocyte with the impaled electrode. Experiments were performed at 20°C with oocytes voltage clamped at -40 mV by using a two-electrode voltage clamp as described previously (6). Oocytes were successively perfused with sodium containing bicarbonate-free oocyte Ringer's solution (82.5 mM NaCl, 2.5 mM KCl, 1 mM

Na<sub>2</sub>HPO<sub>4</sub>, 1 mM MgCl<sub>2</sub>, 1 mM CaCl<sub>2</sub> and 5 mM HEPES, pH 7.4), low-sodium-containing (10% Na<sup>+</sup>, pH 6.4) (8.25 mM NaCl, 75.15 mM NMDG, 2.5 mM KCl, 1 mM Na<sub>2</sub>HPO<sub>4</sub>, 1 mM MgCl<sub>2</sub>, 1 mM CaCl<sub>2</sub> and 5 mM HEPES, pH 6.4), bicarbonate-containing oocyte Ringer's solution (58.5 mM NaCl, 2.5 mM KCl, 1 mM Na<sub>2</sub>HPO<sub>4</sub>, 1 mM MgCl<sub>2</sub>, 1 mM CaCl<sub>2</sub>, 5 mM HEPES and 24 mM NaHCO<sub>3</sub>, pH 7.4, bubbled with 5% CO<sub>2</sub>), and low-sodium and bicarbonate-containing oocyte Ringer's solution (10% Na<sup>+</sup> HCO<sub>3</sub><sup>-</sup>, pH 6.4) (5.85 mM NaCl, 75.15 mM NMDG, 2.5 mM KCl, 1 mM Na<sub>2</sub>HPO<sub>4</sub>, 1 mM MgCl<sub>2</sub>, 1 mM CaCl<sub>2</sub>, 5 mM HEPES and 2.4 mM NaHCO<sub>3</sub>, pH 6.4). Bicarbonate-containing oocyte Ringer's solutions were bubbled continuously with 5% CO<sub>2</sub>-95% O<sub>2</sub>. Changes in membrane current were monitored during 20-mV voltage steps from -100 mV to +20 mV in each solution to obtain current-voltage (*I-V*) curves.

**Bicarbonate transport assays in HEK293 cells.** Briefly, HEK293 cells were grown and transfected on poly-L-lysine-treated 11 × 7.5 mm glass coverslips. Cells were rinsed in serum-free DMEM and incubated in 2 ml of serum-free DMEM containing 2 μM BCECF-AM at 37°C for 15 min. Coverslips were mounted in a fluorescence cuvette and perfused at 3.5 ml/min alternately with Ringer's buffer (5 mM glucose, 5 mM potassium gluconate, 1 mM calcium gluconate, 1 mM MgSO<sub>4</sub>, 2.5 mM NaH<sub>2</sub>PO<sub>4</sub>, 10 mM HEPES, and 25 mM NaHCO<sub>3</sub>, pH 7.4) containing 140 mM NaCl (chloride-containing) or 140 mM sodium gluconate (chloride-free). Both Ringer's buffers were bubbled continuously with air containing 5% CO<sub>2</sub>. Fluorescence was monitored with a Photon Technologies International RCR/Delta Scan spectrofluorimeter at excitation wavelengths of 440 nm and 502.5 nm and emission wavelength of 528.7 nm. Fluorescence measurements were converted to intracellular pH by the nigericin high-potassium method (43) with reference pH values at 6.5, 7.0, and 7.5. Anion exchange activity was calculated by linear regression of the initial 30-s change in intracellular pH upon switching from chloride-containing to a chloride-free Ringer's buffer.  $J_{H^+}$  was calculated as  $J_{H^+} = dpH_i/dt \times (\beta_i + \beta_{CO_2})$  from the slope of the intracellular pH (pH<sub>i</sub>) vs. time fitted curves. Previously determined for HEK293 cells (39), β<sub>i</sub> and β<sub>CO<sub>2</sub></sub> refer to intrinsic and CO<sub>2</sub>/HCO<sub>3</sub><sup>-</sup> buffer capacity (units of mM), respectively.

Sodium-dependent bicarbonate transport experiments were performed by perfusing transfected HEK293 cells (as with Cl<sup>-</sup>/HCO<sub>3</sub><sup>-</sup> exchange assays) with sodium-free Ringer's buffer where NaCl and NaHCO<sub>3</sub> were replaced by choline chloride and choline bicarbonate. Cellular acidification was induced by transient addition and removal of 40 mM NH<sub>4</sub>Cl. Once acidic steady-state pH was established, cells were perfused with Na<sup>+</sup>-containing Ringer's buffer, and the rate of alkalinization was measured during the initial 30 s of recovery from acid load. Buffers were supplemented with ethyl-isopropyl amiloride (EIPA, 5 μM) to inhibit Na<sup>+</sup>/H<sup>+</sup> exchange.

**Preparation of oocyte total membranes.** Oocytes were rinsed and disrupted in Ringer's solution, supplemented with protease inhibitor cocktail by pipetting up and down 20 times. Homogenates were centrifuged at 250 g for 10 min at 4°C to sediment cell debris, and the resulting supernatant was centrifuged at 16,000 g for 20 min at 4°C to produce a membrane-enriched fraction. Pellets were resuspended in Ringer's buffer (2 μl solution/oocyte) containing protease inhibitor cocktail and frozen until use.

**Immunoblots.** Oocyte membrane fraction or HEK293 cell lysates were prepared in SDS-PAGE sample buffer [10% (vol/vol) glycerol, 2% (wt/vol) SDS, 0.5% (wt/vol) bromophenol blue, 75 mM Tris, pH 6.8] containing complete protease inhibitor cocktail. Lysates were made to 1% (vol/vol) 2-mercaptoethanol, heated for 5 min at 65°C, and insoluble material was removed by centrifugation at 16,000 g for 10 min. Samples were resolved by SDS-PAGE on 10% (wt/vol) acrylamide gels (24). Immunoblots were processed as described (45). Mouse anti-HA was used at 1:2,000 dilution in TBS-TM [5% skim milk powder in TBS-T: 0.1% (vol/vol) Tween 20, 0.15 M NaCl, 50 mM Tris·HCl, pH 7.5]. After incubation with sheep antimouse HRP conjugated secondary antibody at 1:5,000 dilution, immunoblots were developed with Millipore Luminata Crescendo Western HRP reagent and visualized by using a GE ImageQuant LAS4000 (GE Healthcare).

**Statistical analysis.** Numerical values are represented as means ± SE. Statistical analysis was performed with Prism software (Graphpad v6). Groups were compared with one-way ANOVA and unpaired *t*-test with *P* < 0.05 considered significant.

**Assessment of borate transport activity.** Plant and yeast SLC4A11 orthologs facilitate borate transport across membranes. One report concluded that human SLC4A11 shares this role (32), which was subsequently questioned (16, 30). *X. laevis* oocytes provide a simple expression system, relatively devoid of transport proteins, to assess transport function. *X. laevis* oocytes were injected with cRNA-encoding human SLC4A11, N-terminal tagged with an HA-epitope. Lysates prepared from SLC4A11 cRNA-injected and noninjected oocytes were analyzed on immunoblots probed with anti-HA antibody. The presence of strong immunoreactivity in cRNA-injected but not in noninjected oocytes reveals SLC4A11 expression (Fig. 1A). SLC4A11 expressed in oocytes migrated as two major bands of 103 and 83 kDa. This migration pattern aligns with that seen for SLC4A11 expressed in HEK293 cells and has been attributed to mature (upper) and immature (lower) glycosylation states of the protein (47).

Oocyte cell swelling was used to monitor borate transport, wherein accumulation of a solute leads to osmotic water movement and cell swelling. Oocytes injected with cRNA encoding the plant major intrinsic protein NIP5;1, established to transport borate (41), swelled upon exposure to iso-osmotic medium, containing 180 mM boric acid (Fig. 1B). The rate of cell swelling was indistinguishable between H<sub>2</sub>O and SLC4A11 cRNA-injected oocytes, but NIP5;1-expressing oocytes had a rate of cell swelling significantly different from H<sub>2</sub>O-injected oocytes (Fig. 1C). These data are consistent with NIP5;1-mediated borate accumulation, leading to osmotic water movement and thus oocyte swelling (41). NIP5;1 therefore exhibits borate transport activity, whereas water-injected oocytes and SLC4A11-expressing oocytes do not. The rate of osmotically driven water movement through NIP5;1 and human SLC4A11 is not statistically different (44). Thus both SLC4A11 and NIP5;1-expressing oocytes have similar water permeabilities. The difference in borate-induced water accumulation rates in NIP5;1 and SLC4A11-expressing oocytes does not therefore arise because of a difference in the capacity of the proteins to facilitate secondary water flux.

Electrogenic Na<sup>+</sup>-coupled boric acid transport was earlier reported for human SLC4A11 expressed in transfected HEK293 cells (32). To assess charge movement associated with SLC4A11 in the presence of borate, SLC4A11-expressing or native oocytes were perfused with oocyte Ringer's buffer, followed by either 1 mM or 5 mM boric acid in oocyte Ringer's buffer while monitoring oocyte current with the two-electrode voltage clamp technique (Fig. 1D). No significant current was induced upon switching to 1 mM or 5 mM borate (Fig. 1E). This indicates that human SLC4A11 does not mediate an electrogenic borate flux.

**Electrophysiology of SLC4A11 water flux.** Human SLC4A11, expressed in HEK293 cells or in *X. laevis* oocytes, was found to induce an increased rate of cell swelling in response to hypo-osmotic challenge (44). Human SLC4A11 was concluded to form a water conductive pathway, with a unitary water flux comparable to the slowest members of the aquaporin family of water channels. To explore the nature of water permeation by SLC4A11, the protein was examined when expressed in *X. laevis* oocytes.

A rapid rise in cell volume followed the switch from iso-osmotic to hypo-osmotic medium for oocytes expressing AQP1 (Fig. 2A), the aquaporin family member with the highest water flux (8). While the rate of oocyte swelling in oocytes expressing human SLC4A11 was significantly slower than AQP1-expressing oocytes (about 35% of AQP1; Fig. 2, A and C), the rate of cell swelling was also significantly faster than in native oocytes.

Since Na<sup>+</sup> has been proposed as a transport substrate of SLC4A11, oocytes were exposed to hypo-osmotic challenge in the presence and absence of Na<sup>+</sup> in the perfusion media (Fig. 2, A and B). The presence of Na<sup>+</sup> did not influence the rate of cell swelling in control oocytes or those expressing AQP1 or SLC4A11 (Fig. 2C).

Similarly, we examined cell-swelling-induced currents in native and SLC4A11-expressing oocytes (Fig. 2, D and E). Switching from iso-osmotic to hypo-osmotic medium induced an inward current flow (i.e., influx of anions or efflux of cations). The magnitude of the current was, however, indistinguishable between native and SLC4A11-expressing oocytes (Fig. 2E).

**Assessment of SLC4A11 pH regulatory activity.** All other members of the SLC4 family are established to be bicarbonate transport proteins (4). Studies of SLC4A11 expressed in mammalian cells suggested that

it does not facilitate bicarbonate transport (16, 30). SLC4A11 has also been proposed to function as a  $\text{Na}^+$ -dependent  $\text{OH}^-$  or  $\text{H}^+$  transporter (19, 30). To explore these transport activities, *X. laevis* oocytes expressing SLC4A11 or “native” oocytes not expressing SLC4A11 were superfused initially with oocyte Ringer's buffer (OR) pH 7.4 in the absence of bicarbonate, while pH was monitored with a  $\text{H}^+$ -selective microelectrode (Fig. 3, A and B). Superfusion with  $\text{CO}_2/\text{HCO}_3^-$ -containing solution, pH 7.4, acidified the oocytes due to  $\text{CO}_2$  diffusion into the cell (Fig. 3, A and B, arrow D). From there a solution containing 10%  $\text{Na}^+$  and  $\text{HCO}_3^-$  at pH 6.4 was introduced, which caused only a small intracellular alkalinization. During this solution change,  $\text{Na}^+$ ,  $\text{HCO}_3^-$ , and  $\text{OH}^-$  gradients were outwardly directed. Switching to OR pH 6.4, containing 10% of normal  $\text{Na}^+$  concentration, established outward-directed  $\text{Na}^+$  and  $\text{OH}^-$  gradients. This led to a slight cytosolic acidification (rise of  $[\text{H}^+]$ , arrow C in Fig. 3, A and B), yet the rate of  $[\text{H}^+]$  change was no different in native or SLC4A11-expressing oocytes (Fig. 3C). This suggests that SLC4A11 does not facilitate  $\text{Na}^+/\text{OH}^-$  transport.

To assess the possibility of  $\text{Na}^+$ -dependent  $\text{HCO}_3^-$  transport by SLC4A11, oocytes were switched from  $\text{Na}^+$ -containing to reduced  $\text{Na}^+$  medium, both in the presence/absence of  $\text{CO}_2/\text{HCO}_3^-$  (Fig. 3, A and B, arrow E). The outward-directed  $\text{Na}^+$  gradient would drive  $\text{HCO}_3^-$  efflux by a  $\text{Na}^+/\text{HCO}_3^-$  cotransporter, resulting in cytosolic acidification. In contrast, both native and SLC4A11-expressing oocytes manifested a slow but indistinguishable alkalinization upon switch to reduced  $\text{Na}^+$  medium (Fig. 3E). This observation is inconsistent with SLC4A11-mediated  $\text{Na}^+/\text{HCO}_3^-$  cotransport.

To detect electrogenic events associated with SLC4A11, currents were measured as native and SLC4A11-expressing oocytes were perfused with the series of solutions described for Fig. 3. While very small currents were detected upon changing perfusion solutions (Fig. 4, A and B), no significant difference in current was observed between the two oocyte types (Fig. 4, C–E). These data indicate that SLC4A11 does not support electrogenic  $\text{Na}^+/\text{OH}^-$  or  $\text{Na}^+/\text{HCO}_3^-$  cotransport.

Since all other SLC4 proteins transport  $\text{HCO}_3^-$ , we further explored whether SLC4A11 functioned in  $\text{Cl}^-/\text{HCO}_3^-$  exchange and  $\text{Na}^+$ -coupled bicarbonate transport activity assays by using transfected HEK293 cells (Fig. 5).  $\text{Cl}^-/\text{HCO}_3^-$  exchange activity was assessed by perfusing initially with  $\text{CO}_2/\text{HCO}_3^-$ -containing Ringer's buffer, followed by  $\text{Cl}^-$ -free Ringer's, and followed by return to  $\text{Cl}^-$ -containing Ringer's while monitoring intracellular pH (Fig. 5A). In cells expressing a functional anion exchanger, removal of  $\text{Cl}^-$  induces cytosolic alkalinization as  $\text{HCO}_3^-$  is brought into the cell in exchange for  $\text{Cl}^-$ . Both vector (pcDNA3.1) and SLC4A11 cDNA transfected cells showed alkalinization following  $\text{Cl}^-$  removal from the medium, consistent with the presence of an anion exchanger (Fig. 5B).

Some SLC4 proteins facilitate  $\text{Na}^+$ -coupled  $\text{HCO}_3^-$  transport (4). To explore this possibility more fully, we also expressed SLC4A11 in transfected HEK293 cells. Cells were acidified, by using the  $\text{NH}_4\text{Cl}$  pulse technique, wherein cells are exposed to medium containing  $\text{NH}_4\text{Cl}$ , inducing alkalinization arising from  $\text{NH}_3$  (a base, in equilibrium with  $\text{NH}_4^+$  in solution) entry into the cytosol (36). Subsequently, medium is exchanged for  $\text{NH}_4\text{Cl}$ -free medium, leading to an outward-directed  $\text{NH}_3$  gradient and  $\text{NH}_3$  efflux. The cytosol then acidifies, overshooting the original resting pH. In  $\text{CO}_2/\text{HCO}_3^-$ -containing medium, the rate of intracellular pH recovery from acid load was monitored in cells treated with the  $\text{Na}^+/\text{H}^+$  exchange inhibitor EIPA (5  $\mu\text{M}$ ) (Fig. 5C). At a range of  $\text{pH}_i$ , the rate of pH change was, however, not different between vector and SLC4A11-transfected HEK293 cells (Fig. 5D).  $\text{Na}^+$ -dependent bicarbonate transport was estimated by  $[\text{H}^+]$  flux ( $J_{\text{H}^+}$ ) during the recovery from acid load at different  $\text{pH}_i$  values. Analysis of  $J_{\text{H}^+}$  revealed no significant difference between vector and SLC4A11-transfected HEK293 cells at any  $\text{pH}_i$  (Fig. 5D). These data are inconsistent with SLC4A11-mediated  $\text{Na}^+/\text{HCO}_3^-$  cotransport.

**Assessment of ammonia transport activity.** A recent report found that human SLC4A11 facilitates  $\text{NH}_3\text{-H}^+$  cotransport when studied in  $\text{Na}^+/\text{H}^+$  exchanger-deficient PS120 cells (50). We further explored the nature of SLC4A11-mediated ammonia transport in an *X. laevis* oocyte expression system. Using double barreled electrodes, we monitored intracellular pH and current in native and SLC4A11-expressing oocytes (Fig. 6). Oocytes were initially perfused with OR, followed by OR containing 10 mM  $\text{NH}_4\text{Cl}$ , and back to OR (Fig. 6, A and B). These superfusions were performed at pH 6.4, 7.4, and 8.4. Since the  $\text{pK}_a$  for  $\text{NH}_4^+$

is 9.4,  $\text{NH}_4^+$  will predominate over  $\text{NH}_3$  in all of these solutions and  $\text{NH}_3$  concentration will increase from pH 6.4 to 8.4. In native oocytes, 10 mM  $\text{NH}_4\text{Cl}$  induced an acidification at all medium pH values studied (Fig. 6A). The rate of acidification progressively rose from pH 6.4 to pH 8.4 (Fig. 6C). The opposite was found for SLC4A11-expressing oocytes (Fig. 6, A and C):  $\text{NH}_4\text{Cl}$  induced an alkalinization, which had the highest rate at pH 8.4. These data are consistent with an endogenous  $\text{NH}_4^+$  translocation pathway in oocytes. Considering the relative amount of  $\text{NH}_3$  and  $\text{NH}_4^+$  being transported, it must be concluded that in native oocytes the transport of  $\text{NH}_4^+$  dominated over  $\text{NH}_3$  transport, whereas in SLC4A11-expressing oocytes the transport of  $\text{NH}_3$  dominated over  $\text{NH}_4^+$  transport.

Effects of  $\text{NH}_4\text{Cl}$  were further explored by measuring the membrane current (Fig. 6, C and D). Little current was observed upon  $\text{NH}_4\text{Cl}$  application at pH 6.4. At pH 7.4 and 8.4, inward currents were induced in both native and SLC4A11-expressing oocytes (Fig. 6D). The current flow was significantly higher in SLC4A11-expressing oocytes than in native oocytes at pH 7.4 and 8.4, and was associated with a robust increase in membrane conductance. With respect to conductance, determined from the slope of the  $I-V$  curves in the presence of 10 mM  $\text{NH}_4\text{Cl}$ , at pH 7.4 native and SLC4A11-expressing oocytes manifested conductance values of  $3.2 \times 10^6$  S and  $8.4 \times 10^6$  S, respectively (Fig. 7). At pH 8.4, these values rose to  $5.5 \times 10^6$  S and  $16.3 \times 10^6$  S for native and SLC4A11 oocytes, respectively. At pH 8.4,  $[\text{H}^+]$  and  $[\text{NH}_4^+]$  are lower than at pH 7.4. Thus the larger conductance in SLC4A11-expressing oocytes is not easily explained by  $\text{NH}_4^+$  or  $\text{NH}_3/\text{H}^+$  conductance through SLC4A11.

Current-voltage ( $I-V$ ) plots associated with  $\text{NH}_4\text{Cl}$  administration (Fig. 7) provided additional insight into SLC4A11-mediated transport. In SLC4A11-expressing oocytes, conductance induced by  $\text{NH}_4\text{Cl}$  is strongly inward rectifying upon membrane hyperpolarization. The observation was highly pH dependent as at pH 6.4 the current is blocked. Plotting the difference in current between SLC4A11-expressing and native oocytes was informative in indicating the contribution of SLC4A11 (Fig. 8). Current flow is enhanced at negative membrane potential, consistent with cation influx or anion efflux. At pH 7.4 and pH 8.4 the reversal potentials were +5.6 mV and -9.5 mV, respectively. This difference in reversal potential with change of pH is in the direction expected for a  $\text{H}^+$ -coupled  $\text{NH}_3$  flux, reported earlier for SLC4A11 expressed in PS120 cells (50). The magnitude of the difference (15 mV) is, however, much smaller than would be calculated were the current due to  $\text{H}^+$  flux, which the Nernst equation calculates as 59 mV.

Finally, we examined the possibility of ammonia transport in by SLC4A11 in transfected HEK293 cells. If SLC4A11 were an ammonia transporter, the  $\text{NH}_4\text{Cl}$  pulse in HEK293 cells (e.g., Fig. 5C) would affect the rate of ammonia equilibration. Cells perfused with  $\text{Na}^+$ -free choline bicarbonate-containing Ringer's buffer were challenged for 3 min with 40 mM  $\text{NH}_4\text{Cl}$  (Fig. 9A). As described above, switching to  $\text{NH}_4\text{Cl}$ -containing medium causes alkalinization, and removal induces acidification (Fig. 9A). To examine the possibility of ammonia transport, we measured the initial steady-state intracellular pH before addition of  $\text{NH}_4\text{Cl}$ , after addition, and after  $\text{NH}_4\text{Cl}$  removal (Fig. 9B). The significantly increased acidification observed in SLC4A11-expressing cells is consistent with enhanced cellular  $\text{NH}_3$  loading and efflux. Intriguingly, the steady-state pH of SLC4A11-expressing cells had a small but significant acidification relative to vector-transfected cells (Fig. 9B,  $\text{pH}_{\text{ini}}$ ). The rate of cytosolic pH change associated with  $\text{NH}_4\text{Cl}$  addition (alkalinization) and removal (acidification) was also quantified (Fig. 9C). SLC4A11-expressing cells have a significantly increased acidification and alkalinization rates, consistent with the  $\text{NH}_3$  transport observed in oocytes. These results suggest that SLC4A11 functions as an  $\text{NH}_3$  transporter when expressed in HEK293 cells.

## DISCUSSION

[Go to:](#)

Mutations of SLC4A11 cause some cases of Fuchs endothelial corneal dystrophy and congenital hereditary endothelial dystrophy, giving rise to profound loss of visual acuity, which are treatable only with corneal transplantation. Knockout mice recapitulate the corneal edema observed in patients with SLC4A11 mutations (13, 27, 44), indicating that the diseases associate with loss of SLC4A11 function. Yet the normal function(s) of SLC4A11 remains uncertain. Before therapeutics can be designed to compensate for loss of SLC4A11 function, we need to understand what is lost in patients carrying SLC4A11 mutations. Here we examined SLC4A11 by using the *X. laevis* oocytes, a system permitting low-background

assessments. We found that SLC4A11 is not a  $\text{HCO}_3^-$  transporter, unlike other members of the SLC4 family. Unlike plant and yeast SLC4A11 orthologs, human SLC4A11 does not support borate transport. Data here provide additional support for  $\text{Na}^+$ -independent, electrically silent water translocation by SLC4A11. Finally, we provide supportive evidence for the recent report that SLC4A11 transports ammonia (50). Unlike the earlier report of  $\text{NH}_3\text{-H}^+$  cotransport, however, we found that SLC4A11 mediates  $\text{NH}_3$  transport without coupled  $\text{H}^+$ .

**Borate transport.** There has been only one report of borate transport by human SLC4A11 (32), and one demonstrated no borate transport by the protein (30). Experiments here failed to find evidence for borate transport by human SLC4A11 when expressed in *X. laevis* oocytes. In contrast, the major intrinsic protein family member protein, NIP5;1, demonstrated borate accumulation as evidenced by solute accumulation-associated cell swelling of oocytes. Oocyte experiments were performed at borate concentrations up to 180 mM. Yet physiological borate levels are unlikely to exceed the 25- $\mu\text{M}$  level observed in the blood of industrially exposed workers (9). Together we could detect no evidence for borate transport by human SLC4A11.

**Water translocation.** Osmotically driven water movement through SLC4A11 was previously observed for the protein expressed in HEK293 cells and *X. laevis* oocytes (44). Data here provided additional confirmation of that observation. Aquaporin proteins, like AQP1, translocate water by forming a “water channel” which directly conducts water. Data here provide additional insight into water movement induced by SLC4A11. Water flux by both SLC4A11 and AQP1 did not require the presence of extracellular  $\text{Na}^+$ . This is consistent with direct movement of  $\text{H}_2\text{O}$ , rather than water flux secondary to  $\text{Na}^+$  movement. Also, no significant current was associated with the water flux associated with SLC4A11 in hypo-osmotically challenged oocytes. This also argues against an indirect mechanism of water movement in which SLC4A11 activates another ion channel or by inducing ion movement itself.

**$\text{NH}_3$  transport.** The observation of  $\text{H}_2\text{O}$  translocation by human SLC4A11 (44) led to experiments to assess possible SLC4A11  $\text{NH}_3/\text{NH}_4^+$  transport function, since some water transporters also mediate transport of the similarly sized substrate  $\text{NH}_3$  (50). Earlier data, collected in  $\text{Na}^+/\text{H}^+$  exchanger-deficient PS120 cells led to the conclusion that SLC4A11 mediates  $\text{NH}_3\text{-H}^+$  cotransport (50). In contrast, our data in oocytes indicate that in the presence of  $\text{NH}_4\text{Cl}$ , SLC4A11 induces cellular alkalization, consistent with  $\text{NH}_3$ , not  $\text{NH}_4^+$  influx. The rate of alkalization increases, moving from medium at pH 6.4 to 8.4, consistent with the increased abundance of  $\text{NH}_3$  with increasing pH. The behavior of SLC4A11-expressing oocytes was in stark contrast with native oocytes, which acidified in  $\text{NH}_4\text{Cl}$ , best explained by  $\text{NH}_4^+$  permeation through endogenous cation channels, driven by the negative membrane potential. Since  $[\text{NH}_4^+]$  decreases further from pH 7.4 to pH 8.4, this indicates that the rate of  $\text{H}^+$  accumulation in native oocytes is not driven solely by  $[\text{NH}_4^+]$ . Perhaps the endogenous  $\text{NH}_4^+$ -conductive pathway alters its  $\text{NH}_4^+$  conductance over the pH 6.4 to 8.4 range.

Additional support for  $\text{NH}_3$  transport by SLC4A11 came from studies in HEK293 cells. The rate of cellular alkalization (from  $\text{NH}_3$  influx) and acidification (from  $\text{NH}_3$  efflux) were both increased in SLC4A11-expressing cells relative to control cells. In addition, SLC4A11-expressing cells shifted their intracellular pH to a greater degree than control cells, following  $\text{NH}_4\text{Cl}$  administration or withdrawal. Again, this is consistent with  $\text{NH}_3$  flux through SLC4A11, but not  $\text{NH}_3\text{-H}^+$  cotransport.

Both native and SLC4A11-expressing oocytes manifested net anion entry or cation efflux in the presence of  $\text{NH}_4\text{Cl}$ . The current was higher at pH 7.4 and 8.4 than pH 6.4. The presence of an inward current in native oocytes, although of a lesser magnitude than in SLC4A11-expressing oocytes, suggests that the current arises from an oocyte-endogenous process. The reason why current and conductance increase are larger in SLC4A11-expressing oocytes is unclear. One possibility is that in the presence of  $\text{NH}_4\text{Cl}$  native oocytes acidify, whereas SLC4A11-expressing oocytes alkalize (which was observed). The conductance observed in SLC4A11-expressing oocytes might arise because of alkalization-dependent opening of oocyte-endogenous channels.

Importantly, we do note that the conductance that we observed is similar to that observed for SLC4A11 expressed in PS120 cells, which was earlier interpreted as arising from coupled  $\text{NH}_3/\text{H}^+$  flux (50). Little

can be concluded about the nature of the membrane conductance increase and the small shift in reversal potential between pH 6.4 and 8.4 (Fig. 8). Examination of the net current present in SLC4A11-expressing oocytes (current in SLC4A11 expressing minus current in native oocytes) (Fig. 8) reveals little current in the absence of  $\text{NH}_4\text{Cl}$ . The shift of 15 mV between solutions buffered to pH 7.4 and 8.4 (Fig. 8) makes it unlikely that there is a major contribution of  $\text{H}^+$ . The most likely candidates for the ionic conductance change are either  $\text{Cl}^-$  or  $\text{K}^+$  channels, which are endogenously present in *Xenopus* oocytes (42, 48). If so, the data suggest that the endogenous oocyte channels are gated open at alkaline pH (pH 7.4/8.4) and close at acidic (pH 6.4). The current would be consistent with an  $\text{NH}_4^+$  flux, since the current is depolarizing. Against this possibility, SLC4A11-expressing oocytes clearly alkalinize in the presence of  $\text{NH}_4\text{Cl}$ , which is opposite what one would expect if  $\text{NH}_4^+$  were to enter the cell. Moreover,  $\text{NH}_4^+$  concentration is higher at pH 6.4 than 7.4, but we observe much more current at pH 7.4 (Fig. 7D). One final way to reconcile the data is combined  $\text{NH}_4^+$  and  $\text{NH}_3$  influx, with a predominance of  $\text{NH}_3$ . This would be consistent with the SLC4A11-mediated  $\text{NH}_3/2\text{H}^+$  transport observed in PS120 cells (50) and explain the net alkalinization observed. This explanation would hold true only if SLC4A11 was poorly  $\text{NH}_4^+$  permeable at acidic pH.

In reviewing the evidence, we find that pH changes associated with  $\text{NH}_4\text{Cl}$  addition and removal, in both oocytes and HEK293 cells, are consistent with  $\text{NH}_3$ , not  $\text{NH}_3/\text{H}^+$  flux mediated by SLC4A11. The only evidence here potentially consistent with  $\text{NH}_3\text{-H}^+$  cotransport by SLC4A11 is net current associated with  $\text{NH}_4\text{Cl}$  administration in oocytes. On balance we find that the evidence favors  $\text{NH}_3$  transport by SLC4A11, but we cannot completely rule out  $\text{NH}_3\text{-H}^+$  cotransport.

$\text{NH}_3$  permeation by SLC4A11 introduces interesting physiological implications. Corneal endothelial cells were proposed to produce significant amounts of waste ammonia through preferential use of glutamine deamidation as an energy source (50). Although the present study and earlier work examined SLC4A11 handling of extracellular ammonia, in corneal endothelium the protein would function in ammonia efflux. In the corneal endothelium, SLC4A11 is basolateral, facing the corneal stroma and front of the eye. Waste ammonia moved into the stroma could diffuse through the stroma to the eye's surface epithelium. The presence of SLC4A11 in the epithelium could assist in efflux of  $\text{NH}_3$  from epithelium to the air.

As discussed earlier (50), a role for SLC4A11 in renal physiology should also be considered, since the protein localizes to the thin descending limb (TDL) of the loop of Henle (13). Basolaterally located SLC4A11 in the TDL is ideally located to facilitate the movement of  $\text{NH}_3$  from the medullary interstitium into the lumen as part of the ammonia recycling mechanism concentrating ammonia in the medullary interstitium (49). This defect would impair the ability of *slc4a11*<sup>-/-</sup> mice to acidify their urine in response to an acid load. SLC4A11 may also play a role in moving water across the TDL, a process essential to the counter-current multiplier mechanism, permitting the concentration of urine. Consistent with this possibility a reduction in this water flux could contribute to the increased urinary osmolarity and polyuria observed in *slc4a11*<sup>-/-</sup> mice (13).

**pH Regulatory transporter.** Except for SLC4A11, all other SLC4 family members are bicarbonate transporters (4). Here we found that SLC4A11 expressed in oocytes did not support  $\text{HCO}_3^-$ -dependent recovery from acid load, whether  $\text{Na}^+$  was present in the medium or not. We also found that SLC4A11 expressed in HEK293 cells did not support a level of  $\text{Cl}^-/\text{HCO}_3^-$  exchange activity or  $\text{Na}^+\text{-HCO}_3^-$  cotransport that was different from vector-transfected cells. Together these data do not provide support for bicarbonate transport by human SLC4A11. These data are consistent with the lack of  $\text{HCO}_3^-$  transport function observed previously for SLC4A11 in HEK293 cells (30) or in corneal endothelial cells (16).

Earlier reports found  $\text{H}^+$  or  $\text{OH}^-$  transport by SLC4A11 (16, 19). HEK293 cells were hyperpolarized by manipulation of extracellular  $\text{K}^+$  or  $\text{Na}^+$  concentrations, which led to greater rates of acidification in SLC4A11-expressing cells than in control cells, consistent with  $\text{H}^+$  influx or  $\text{OH}^-$  efflux (19). These data suggest that in addition to water permeation, SLC4A11 can facilitate  $\text{H}^+$  or  $\text{OH}^-$  movement, driven by the membrane potential. In voltage clamp experiments, we monitored the difference in current between SLC4A11-expressing and control oocytes, which revealed very little current, even at  $-100$  mV in the absence of  $\text{NH}_4\text{Cl}$  (Fig. 9). These data do not support voltage-driven  $\text{H}^+$  or  $\text{OH}^-$  transport by SLC4A11. Earlier reports (16, 19) of  $\text{H}^+$  or  $\text{OH}^-$  movement through SLC4A11 may reflect their use of mammalian

cell expression systems (HEK293 or PS120 cells). Consistent with this possibility, we found that SLC4A11 expression induced a small but significant decrease in HEK293 cell baseline intracellular pH (Fig. 9B,  $\text{pH}_{\text{ini}}$ ), an observation found in earlier studies of SLC4A11 in PS120 cells (50). Together, we suggest that SLC4A11 either 1) activates  $\text{H}^+$  equivalent flux through a protein endogenous to mammalian cells but not oocytes, or 2) some cofactor (protein) is absent from oocytes that is required for  $\text{H}^+$  equivalent flux through SLC4A11.

**SLC4A11 isoform-specific functions.** Three SLC4A11 transcript splicing variants have been reported, which differ in their N-terminal cytoplasmic sequences and have been called variants a, b, c or 1, 2, 3 (19). Recently, splice form 3 was reported as the only transcript present in human corneal cells (19). In contrast, we found that splices form 2 and 3 are present in both whole cornea and microdissected corneal endothelium (Darpan Malhotra, unpublished observations). Recent studies suggested that the SLC4A11 cytoplasmic and integral membrane domains are intimately associated and that the cytoplasmic domain contributes to the transport function of SLC4A11 (26). Variations at the N-terminus could thus affect SLC4A11 function or regulation. We found that the translational initiation for splice form 2 is at the second Met of the coding sequence. Consequently, the only difference between splice form 2 and 3 is a unique 19 amino acid N-terminal extension on splice form 3. One observation of  $\text{H}^+/\text{OH}^-$  transport used splice form 3, and the suggestion was made that splice form 2, studied in the present paper, may function in water translocation, whereas splice form 3 may be a  $\text{H}^+/\text{OH}^-$  transporter (19). On the other hand, splice form 2 was also reported to mediate  $\text{H}^+/\text{OH}^-$  transport (30), indicating that this activity is not exclusive to splice form 3. This latter study monitored pH recovery from  $\text{NH}_4\text{Cl}$ -induced acid load as a measure of SLC4A11 function. Although rates of intracellular pH recovery were performed in the nominal absence of  $\text{NH}_4\text{Cl}$ , the alkalinizing activity observed may have likely resulted from SLC4A11-mediated transport of the base  $\text{NH}_3$  into the cell.

**Conclusions.** Here we provided the first comprehensive examination of the reported functional activities of SLC4A11, a plasma membrane transport protein mutated in corneal dystrophies. Studies were undertaken to examine human SLC4A11 functions for the first time (except for water flux) in *X. laevis* oocytes. Although SLC4A11 is a member of the SLC4 family of bicarbonate transporters, we could find no evidence for this activity. Similarly, although SLC4A11 orthologs in other species transport borate, human SLC4A11 does not. When expressed in oocytes, SLC4A11 is not a voltage-driven  $\text{H}^+$  or  $\text{OH}^-$  transporter. Earlier suggestions of this activity may reflect that additional proteins present in mammalian cells are needed to observe the function. Studies in oocytes and mammalian cells provide support for SLC4A11-mediated  $\text{NH}_3$  transport, but not  $\text{NH}_3\text{-H}^+$  cotransport. Water flux and  $\text{NH}_3$  transport functions of SLC4A11 are  $\text{Na}^+$  independent and electroneutral.

## GRANTS

[Go to:](#)

Operating support was provided by Canadian Institutes of Health Research (to J. R. Casey) and by Deutsche Forschungsgemeinschaft Grant DE 231/24-2 (to J. W. Deitmer). S. L. Loganathan was supported by a graduate studentship from the Natural Sciences and Engineering Research Council (Canada)-supported International Research Training Group in Membrane Biology.

## DISCLOSURES

[Go to:](#)

No conflicts of interest, financial or otherwise, are declared by the author(s).

## AUTHOR CONTRIBUTIONS

[Go to:](#)

S.K.L., P.E.M., J.W.D., and J.R.C. conception and design of research; S.K.L., H.-P.S., and P.E.M. performed experiments; S.K.L., H.-P.S., P.E.M., J.W.D., and J.R.C. analyzed data; S.K.L., P.E.M., J.W.D., and J.R.C. interpreted results of experiments; S.K.L., H.-P.S., P.E.M., and J.R.C. prepared figures; S.K.L. and J.R.C. drafted manuscript; S.K.L., P.E.M., J.W.D., and J.R.C. edited and revised manuscript; S.K.L., H.-P.S., P.E.M., J.W.D., and J.R.C. approved final version of manuscript.

## ACKNOWLEDGMENTS

[Go to:](#)

We thank Deborah O'Neill and Dr. Chris Cheeseman for providing *X. laevis* oocytes.

## REFERENCES

Go to:

1. Aldahmesh MA, Khan AO, Meyer BF, Alkuraya FS. Mutational spectrum of SLC4A11 in autosomal recessive CHED in Saudi Arabia. *Invest Ophthalmol Vis Sci* 50: 4142–4145, 2009. [PubMed: 19369245]
2. Aldave AJ, Han J, Frausto RF. Genetics of the corneal endothelial dystrophies: an evidence-based review. *Clin Genet* 84: 109–119, 2013. [PMCID: PMC3885339] [PubMed: 23662738]
3. Aldave AJ, Yellore VS, Bourla N, Momi RS, Khan MA, Salem AK, Rayner SA, Glasgow BJ, Kurtz I. Autosomal recessive CHED associated with novel compound heterozygous mutations in SLC4A11. *Cornea* 26: 896–900, 2007. [PubMed: 17667634]
4. Alka K, Casey JR. Bicarbonate transport in health and disease. *IUBMB Life* 66: 596–615, 2014. [PubMed: 25270914]
5. Becker HM, Broer S, Deitmer JW. Facilitated lactate transport by MCT1 when coexpressed with the sodium bicarbonate cotransporter (NBC) in *Xenopus* oocytes. *Biophys J* 86: 235–247, 2004. [PMCID: PMC1303786] [PubMed: 14695265]
6. Becker HM, Deitmer JW. Carbonic anhydrase II increases the activity of the human electrogenic  $\text{Na}^+/\text{HCO}_3^-$  cotransporter. *J Biol Chem* 282: 13508–13521, 2007. [PubMed: 17353189]
7. Bonanno JA. Molecular mechanisms underlying the corneal endothelial pump. *Exp Eye Res* 95: 2–7, 2012. [PMCID: PMC3199349] [PubMed: 21693119]
8. Borgnia M, Nielsen S, Engel A, Agre P. Cellular and molecular biology of the aquaporin water channels. *Annu Rev Biochem* 68: 425–458, 1999. [PubMed: 10872456]
9. Culver BD, Shen PT, Taylor TH, Lee-Feldstein A, Anton-Culver H, Strong PL. The relationship of blood- and urine-boron to boron exposure in borax-workers and usefulness of urine-boron as an exposure marker. *Environ Health Perspect* 102 Suppl 7: 133–137, 1994. [PMCID: PMC1566651]
10. Damkier HH, Nielsen S, Praetorius J. Molecular expression of SLC4 derived  $\text{Na}^+$  dependent anion transporters in selected human tissues. *Am J Physiol Regul Integr Comp Physiol* 293: R2136–R2146, 2007. [PubMed: 17715183]
11. Deitmer JW. Electrogenic sodium-dependent bicarbonate secretion by glial cells of the leech central nervous system. *J Gen Physiol* 98: 637–655, 1991. [PMCID: PMC2229066] [PubMed: 1761972]
12. Desir J, Moya G, Reish O, Van Regemorter N, Deconinck H, David KL, Meire FM, Abramowicz M. Borate transporter SLC4A11 mutations cause both Harboyan syndrome and non-syndromic corneal endothelial dystrophy. *J Med Genet* 44: 322–326, 2007. [PMCID: PMC2597979] [PubMed: 17220209]
13. Groeger N, Froehlich H, Maier H, Olbrich A, Kostin S, Braun T, Boettger T. Slc4a11 prevents osmotic imbalance leading to corneal endothelial dystrophy, deafness, and polyuria. *J Biol Chem* 285: 14467–14474, 2010. [PMCID: PMC2863209] [PubMed: 20185830]
14. Hemadevi B, Veitia RA, Srinivasan M, Arunkumar J, Prajna NV, Lesaffre C, Sundaresan P. Identification of mutations in the SLC4A11 gene in patients with recessive congenital hereditary endothelial dystrophy. *Arch Ophthalmol* 126: 700–708, 2008. [PubMed: 18474783]
16. Jalimarada SS, Ogando DG, Vithana EN, Bonanno JA. Ion transport function of SLC4A11 in corneal endothelium. *Invest Ophthalmol Vis Sci* 54: 4330–4340, 2013. [PMCID: PMC3691053] [PubMed: 23745003]
17. Jennings ML, Howren TR, Cui J, Winters MJ, Hannigan R. Transport and regulatory characteristics of the yeast bicarbonate transporter homolog Bor1p. *Am J Physiol Cell Physiol* 293: C468–C476, 2007. [PubMed: 17459946]
18. Jiao X, Sultana A, Garg P, Ramamurthy B, Vemuganti GK, Gangopadhyay N, Hejtmancik JF, Kannabiran C. Autosomal recessive corneal endothelial dystrophy (CHED2) is associated with mutations

- in SLC4A11. *J Med Genet* 44: 64–68, 2007. [PMCID: PMC2597914] [PubMed: 16825429]
19. Kao L, Azimov R, Abuladze N, Newman D, Kurtz I. Human SLC4A11-C functions as a DIDS-stimulatable  $H^+(OH^-)$  permeation pathway: partial correction of R109H mutant transport. *Am J Physiol Cell Physiol* 308: C176–C188, 2015. [PMCID: PMC4297769] [PubMed: 25394471]
  20. Kaul H, Suman M, Khan Z, Ullah MI, Ashfaq UA, Idrees S. Missense mutation in SLC4A11 in two Pakistani families affected with congenital hereditary endothelial dystrophy (CHED2). *Clin Exp Optom* 99: 73–77, 2015. [PubMed: 26286922]
  21. Klintworth GK. Corneal dystrophies. *Orphanet J Rare Dis* 4: 7, 2009. [PMCID: PMC2695576] [PubMed: 19236704]
  22. Kodaganur SG, Kapoor S, Veerappa AM, Tontanahal SJ, Sarda A, Yathish S, Prakash DR, Kumar A. Mutation analysis of the SLC4A11 gene in Indian families with congenital hereditary endothelial dystrophy 2 and a review of the literature. *Mol Vis* 19: 1694–1706, 2013. [PMCID: PMC3733908] [PubMed: 23922488]
  23. Kumar A, Bhattacharjee S, Prakash DR, Sadanand CS. Genetic analysis of two Indian families affected with congenital hereditary endothelial dystrophy: two novel mutations in SLC4A11. *Mol Vis* 13: 39–46, 2007. [PMCID: PMC2503190] [PubMed: 17262014]
  24. Laemmli UK. Cleavage of structural proteins during assembly of the head of bacteriophage T4. *Nature* 227: 680–685, 1970. [PubMed: 5432063]
  25. Loganathan SK, Casey JR. Corneal dystrophy-causing SLC4A11 mutants: suitability for folding-correction therapy. *Hum Mutat* 35: 1082–1091, 2014. [PubMed: 24916015]
  26. Loganathan SK, Lukowski CM, Casey JR. The cytoplasmic domain is essential for transport function of the integral membrane transport protein SLC4A11. *Am J Physiol Cell Physiol* 310: C161–C174, 2016. [PMCID: PMC4719032] [PubMed: 26582474]
  27. Lopez IA, Rosenblatt MI, Kim C, Galbraith GG, Jones SM, Kao L, Newman D, Liu W, Yeh S, Pushkin A, Abuladze N, Kurtz I. Slc4a11 gene disruption in mice: cellular targets of sensorineuronal abnormalities. *J Biol Chem* 28: 26882–26896, 2009. [PMCID: PMC2785376]
  28. Munsch T, Deitmer JW. Sodium-bicarbonate cotransport current in identified leech glial cells. *J Physiol* 474: 43–53, 1994. [PMCID: PMC1160294] [PubMed: 8014897]
  29. Noguchi K, Yasumori M, Imai T, Naito S, Matsunaga T, Oda H, Hayashi H, Chino M, Fujiwara T. Bor1-1, an Arabidopsis thaliana mutant that requires a high level of boron. *Plant Physiol* 115: 901–906, 1997. [PMCID: PMC158553] [PubMed: 9390427]
  30. Ogando DG, Jalimarada SS, Zhang W, Vithana EN, Bonanno JA. SLC4A11 is an EIPA-sensitive  $Na^+$  permeable pHi regulator. *Am J Physiol Cell Physiol* 305: C716–C727, 2013. [PMCID: PMC3798668] [PubMed: 23864606]
  31. O'Neill MA, Ishii T, Albersheim P, Darvill AG. Rhamnogalacturonan II: structure and function of a borate cross-linked cell wall pectic polysaccharide. *Annu Rev Plant Biol* 55: 109–139, 2004. [PubMed: 15377216]
  - 31a. Online Mendelian Inheritance in Man. Corneal dystrophy, Fuchs endothelial, late-onset. In: Online Mendelian Inheritance in Man. An Online Catalog of Human Genes and Genetic Disorders. Baltimore, MD: Johns Hopkins University. MIM Number: 610158; <http://omim.org/> [Sept. 13, 2016].
  32. Park M, Li Q, Shcheynikov N, Zeng W, Muallem S. NaBC1 is a ubiquitous electrogenic  $Na^+$ -coupled borate transporter essential for cellular boron homeostasis and cell growth and proliferation. *Mol Cell* 16: 331–341, 2004. [PubMed: 15525507]
  33. Patel SP, Parker MD. SLC4A11 and the pathophysiology of congenital hereditary endothelial dystrophy. *Biomed Res Int* 2015: 475392, 2015. [PMCID: PMC4588344] [PubMed: 26451371]

34. Puangsricharern V, Yeetong P, Charumalai C, Suphapeetiporn K, Shotelersuk V. Two novel mutations including a large deletion of the SLC4A11 gene causing autosomal recessive hereditary endothelial dystrophy. *Br J Ophthalmol* 98: 1460–1462, 2014. [PubMed: 25138764]
35. Ramprasad VL, Ebenezer ND, Aung T, Rajagopal R, Yong VH, Tuft SJ, Viswanathan D, El-Ashry MF, Liskova P, Tan DT, Bhattacharya SS, Kumaramanickavel G, Vithana EN. Novel SLC4A11 mutations in patients with recessive congenital hereditary endothelial dystrophy (CHED2). *Mutation in brief* #958. Online. *Hum Mutat* 28: 522–523, 2007.
36. Roos A, Boron WF. Intracellular pH. *Physiol Rev* 61: 296–434, 1981. [PubMed: 7012859]
37. Siddiqui S, Zenteno JC, Rice A, Chacon-Camacho O, Naylor SG, Rivera-de la Parra D, Spokes DM, James N, Toomes C, Inglehearn CF, Ali M. Congenital hereditary endothelial dystrophy caused by SLC4A11 mutations progresses to Harboyan syndrome. *Cornea* 33: 247–251, 2014. [PMCID: PMC4195577] [PubMed: 24351571]
38. Soumitra N, Loganathan SK, Madhavan D, Ramprasad VL, Arokiasamy T, Sumathi S, Karthiyayini T, Rachapalli SR, Kumaramanickavel G, Casey JR, Rajagopal R. Biosynthetic and functional defects in newly identified SLC4A11 mutants and absence of COL8A2 mutations in Fuchs endothelial corneal dystrophy. *J Hum Genet* 59: 444–453, 2014. [PubMed: 25007886]
39. Sterling D, Casey JR. Transport activity of AE3 chloride/bicarbonate anion-exchange proteins and their regulation by intracellular pH. *Biochem J* 344: 221–229, 1999. [PMCID: PMC1220634] [PubMed: 10548554]
40. Sultana A, Garg P, Ramamurthy B, Vemuganti GK, Kannabiran C. Mutational spectrum of the SLC4A11 gene in autosomal recessive congenital hereditary endothelial dystrophy. *Mol Vis* 13: 1327–1332, 2007. [PubMed: 17679935]
41. Takano J, Wada M, Ludewig U, Schaaf G, von Wiren N, Fujiwara T. The Arabidopsis major intrinsic protein NIP5;1 is essential for efficient boron uptake and plant development under boron limitation. *Plant Cell* 18: 1498–1509, 2006. [PMCID: PMC1475503] [PubMed: 16679457]
42. Terhag J, Cavara NA, Hollmann M. Cave canalem: how endogenous ion channels may interfere with heterologous expression in *Xenopus* oocytes. *Methods* 51: 66–74, 2010. [PubMed: 20123125]
43. Thomas JA, Buchsbaum RN, Zimniak A, Racker E. Intracellular pH measurements in Ehrlich ascites tumor cells utilizing spectroscopic probes generated in situ. *Biochemistry* 18: 2210–2218, 1979. [PubMed: 36128]
44. Vilas GL, Loganathan SK, Liu J, Riau AK, Young JD, Mehta JS, Vithana EN, Casey JR. Transmembrane water-flux through SLC4A11: a route defective in genetic corneal diseases. *Hum Mol Genet* 22: 4579–4590, 2013. [PMCID: PMC3889808] [PubMed: 23813972]
45. Vilas GL, Morgan PE, Loganathan S, Quon A, Casey JR. A biochemical framework for SLC4A11, the plasma membrane protein defective in corneal dystrophies. *Biochem J* 50: 2157–2169, 2011.
46. Vithana EN, Morgan P, Sundaresan P, Ebenezer ND, Tan DT, Mohamed MD, Anand S, Khine KO, Venkataraman D, Yong VH, Salto-Tellez M, Venkataraman A, Guo K, Hemadevi B, Srinivasan M, Prajna V, Khine M, Casey JR, Inglehearn CF, Aung T. Mutations in sodium-borate cotransporter SLC4A11 cause recessive congenital hereditary endothelial dystrophy (CHED2). *Nat Genet* 38: 755–757, 2006. [PubMed: 16767101]
47. Vithana EN, Morgan PE, Ramprasad V, Tan DT, Yong VH, Venkataraman D, Venkataraman A, Yam GH, Nagasamy S, Law RW, Rajagopal R, Pang CP, Kumaramanickavel G, Casey JR, Aung T. SLC4A11 mutations in Fuchs endothelial corneal dystrophy (FECD). *Hum Mol Genet* 17: 656–666, 2008. [PubMed: 18024964]
48. Weber WM. Endogenous ion channels in oocytes of *Xenopus laevis*: recent developments. *J Membr Biol* 170: 1–12, 1999. [PubMed: 10398755]

49. Weiner ID, Verlander JW. Role of  $\text{NH}_3$  and  $\text{NH}_4^+$  transporters in renal acid-base transport. *Am J Physiol Renal Physiol* 300: F11–F23, 2011. [PMCID: PMC3023229] [PubMed: 21048022]

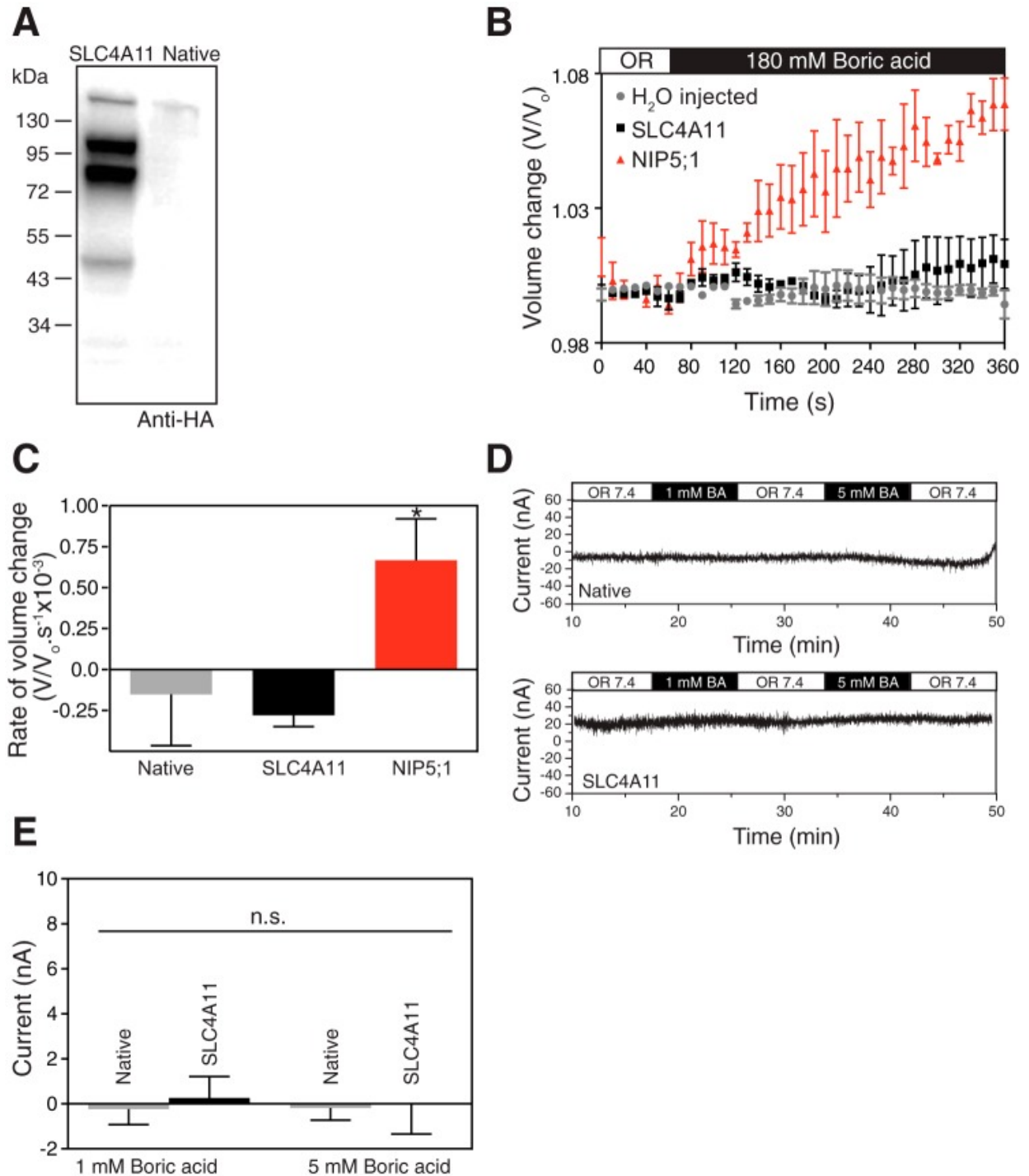
50. Zhang W, Ogando DG, Bonanno JA, Obukhov AG. Human SLC4A11 is a novel  $\text{NH}_3/\text{H}^+$  co-transporter. *J Biol Chem* 290: 16894–16905, 2015. [PMCID: PMC4505435] [PubMed: 26018076]

## **Figures and Tables**

[Go to:](#)

---

**Fig. 1.**

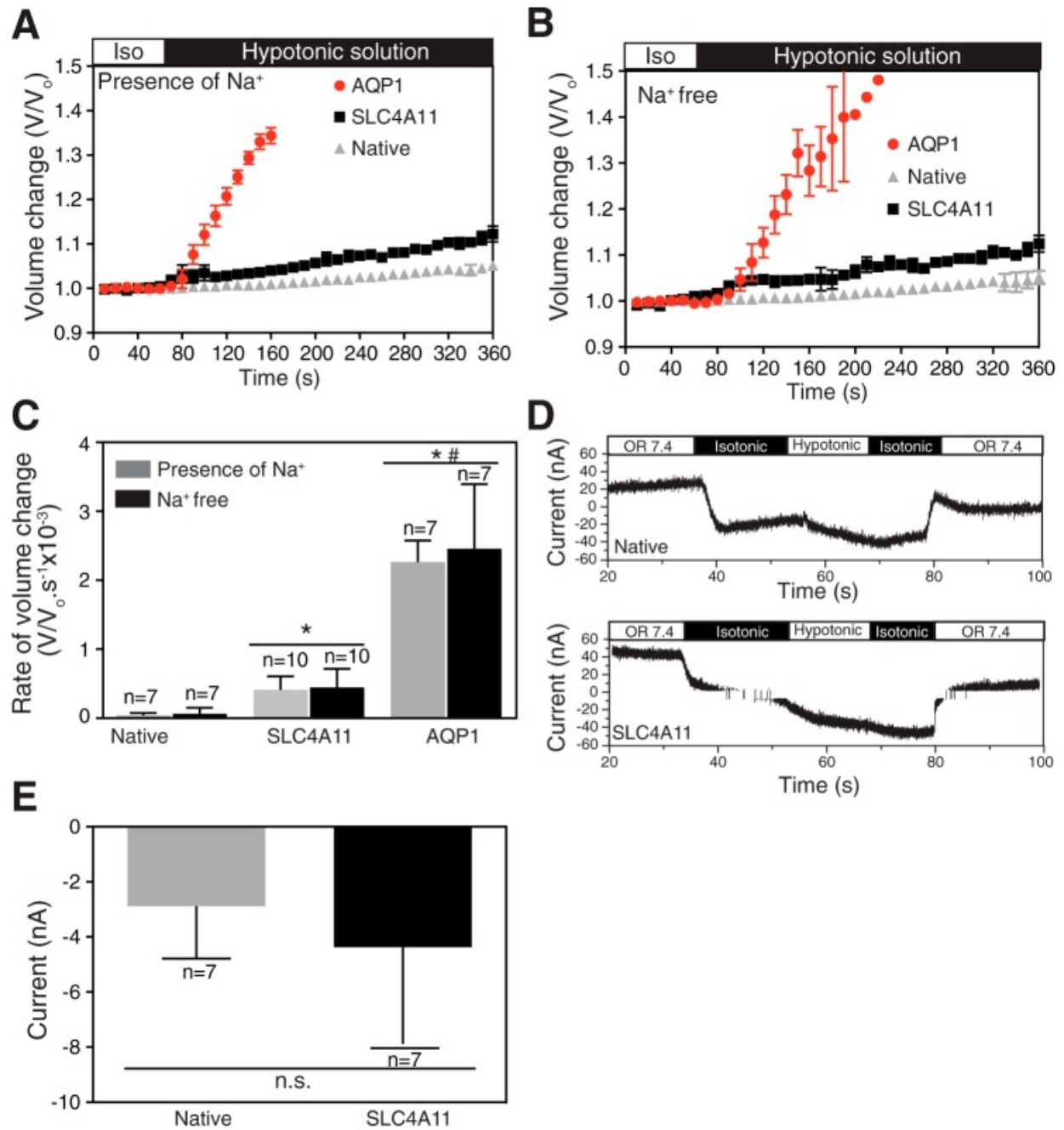


[Open in a separate window](#)

SLC4A11 does not transport borate. *A*: cRNA-encoding N-terminally HA-epitope tagged SLC4A11 or water-injected *X. laevis* oocytes were incubated for 72 h. Oocytes were fractionated to isolate the membrane-rich fractions, and the samples were processed for immunoblotting with anti-HA antibody. *B*: borate transport was measured in oocytes by using an assay reported earlier (41). When borate enters the oocyte, osmolarity increases and water crosses the oocyte membrane to maintain transmembrane isoosmolarity. SLC4A11 or NIP5;1 cRNA or water-injected oocytes were incubated for 72 h and exposed to oocyte Ringer's (OR, white bar) solution (220 mosM/kg) for 1 min. Oocytes were then switched to OR isotonic solution containing 180 mM borate solution (black bar), while continuously monitoring under microscope and capturing images digitally every 15 s. Volume change was calculated by normalizing to average volume during initial 60 s. *C*: rate of volume change was represented by calculating the slope of initial swelling after switching to 180 mM borate solution. *D*: SLC4A11 cRNA-injected or native oocytes were incubated for 72 h and current was measured with a single-barreled microelectrode while perfusing the oocytes with oocyte Ringer's solution (OR 7.4, white bar), OR containing 1 mM borate solution (1 mM BA, black bar), and OR containing 5 mM borate solution (5 mM BA, black bar). *E*: SLC4A11-mediated membrane current, induced by switching to 1 mM or 5 mM borate solution is shown for native oocytes or SLC4A11

expressing oocytes. Error bars represent means  $\pm$  SE ( $n = 7-10$ ); \*significant difference from H<sub>2</sub>O injected oocytes ( $P < 0.05$ ); n.s., not significant.

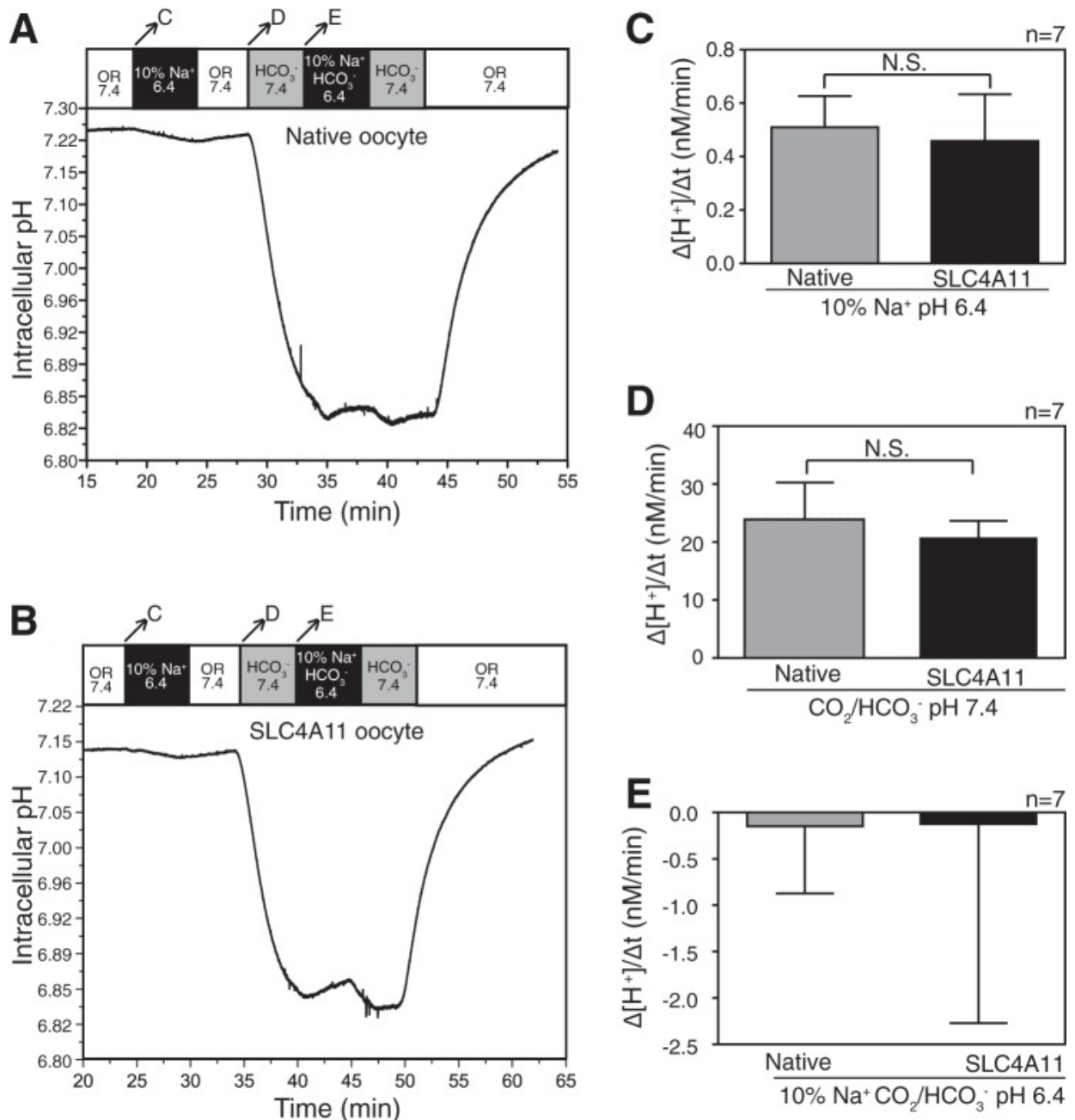
**Fig. 2.**



[Open in a separate window](#)

SLC4A11 mediates osmotic (independent of Na<sup>+</sup>) and electroneutral water movement in oocytes. *A* and *B*: oocytes (injected with cRNA-encoding N-terminally HA-epitope tagged SLC4A11 or AQP1 cRNA) were perfused with 220 mosM/kg isotonic oocyte ND96 medium (white bar), followed by 44 mosM/kg hypotonic solution (black bar). Perfusions proceeded in the absence (*B*) (replaced by choline chloride) or presence (*A*) of 96 mM NaCl. *C*: oocyte volume was calculated from images captured digitally every 15 s. Rate of volume change was represented by calculating the slope of initial swelling after switching to hypotonic solution. *D*: whole cell current was measured, with a single-barreled microelectrode, in oocytes injected with SLC4A11 cRNA or native oocytes. Oocytes were perfused with oocyte Ringer's solution (OR 7.4, white bar), 220 mosM/kg solution (isotonic, black bar), and 44 mosM/kg solution (hypotonic, white bar). *E*: SLC4A11 mediated membrane current, induced by switching from isotonic to hypotonic medium was determined for oocytes, during the first switch to hypo-osmotic medium. Error bars represent means ± SE ( $n = 7-10$ ); \*significant difference from H<sub>2</sub>O-injected oocytes; #significant difference from SLC4A11-injected oocytes ( $P < 0.05$ ); n.s., not significant.

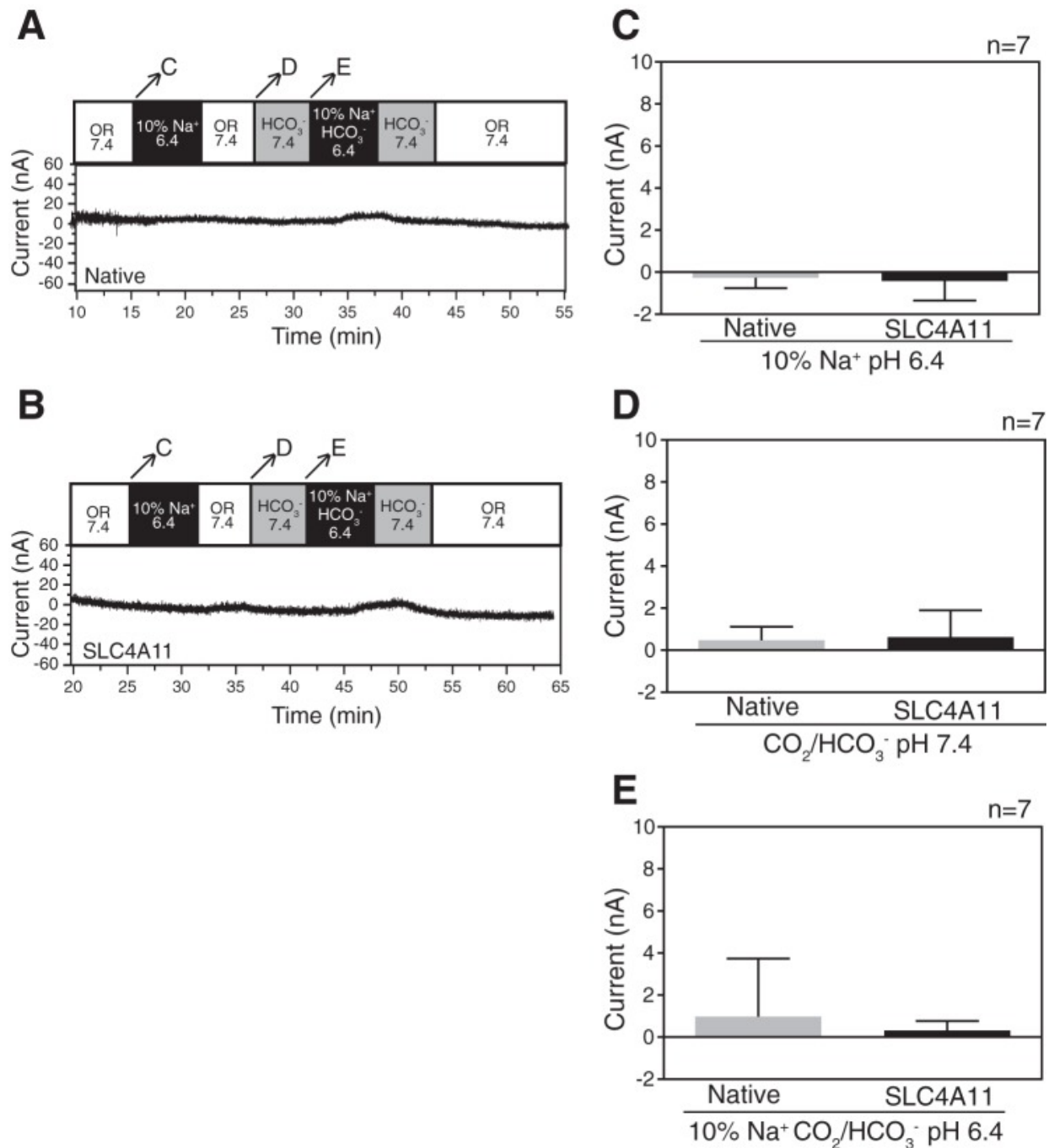
**Fig. 3.**



[Open in a separate window](#)

Assessment of SLC4A11-mediated Na<sup>+</sup> dependent or independent H<sup>+</sup>/OH<sup>-</sup>/HCO<sub>3</sub><sup>-</sup> pH change in oocytes. SLC4A11 cRNA-injected or native oocytes were incubated for 72 h. pH and current were simultaneously measured with a double-barreled microelectrode combined with a two-electrode voltage clamp (clamped to -40 mV). *A* and *B*: cytosolic pH was measured as native (*A*) or SLC4A11-expressing (*B*) oocytes and were sequentially superfused with oocyte Ringer's solution containing 82.5 mM NaCl (OR 7.4, white bar), oocyte Ringer's solution containing only 5.85 mM NaCl (total [Na<sup>+</sup>] 10% of OR), and 2.4 mM HCO<sub>3</sub><sup>-</sup>, adjusted to pH 6.4 (10% Na<sup>+</sup> HCO<sub>3</sub><sup>-</sup>, 6.4, black bar). Bicarbonate and bicarbonate-free oocyte Ringer's solutions were bubbled continuously with 5% CO<sub>2</sub>-95% O<sub>2</sub>. Arrows across the top bar indicate the time period when rates of pH change were measured, and the corresponding letters indicate the panel with the rates compared. *C*: Na<sup>+</sup> dependent H<sup>+</sup>/OH<sup>-</sup> ion movement mediated by SLC4A11 was calculated from rate of change of intracellular [H<sup>+</sup>] when oocytes were switched from OR 7.4 to 10% Na<sup>+</sup>, pH 6.4. *D* and *E*: Na<sup>+</sup> independent or dependent bicarbonate movement mediated by SLC4A11 was calculated from rate of change in [H<sup>+</sup>]<sub>i</sub> concentration when oocytes were switched from OR 7.4 to HCO<sub>3</sub><sup>-</sup> 7.4 and then to 10% Na<sup>+</sup> and HCO<sub>3</sub><sup>-</sup>, pH 6.4. Error bars represent means ± SE (*n* = 7).

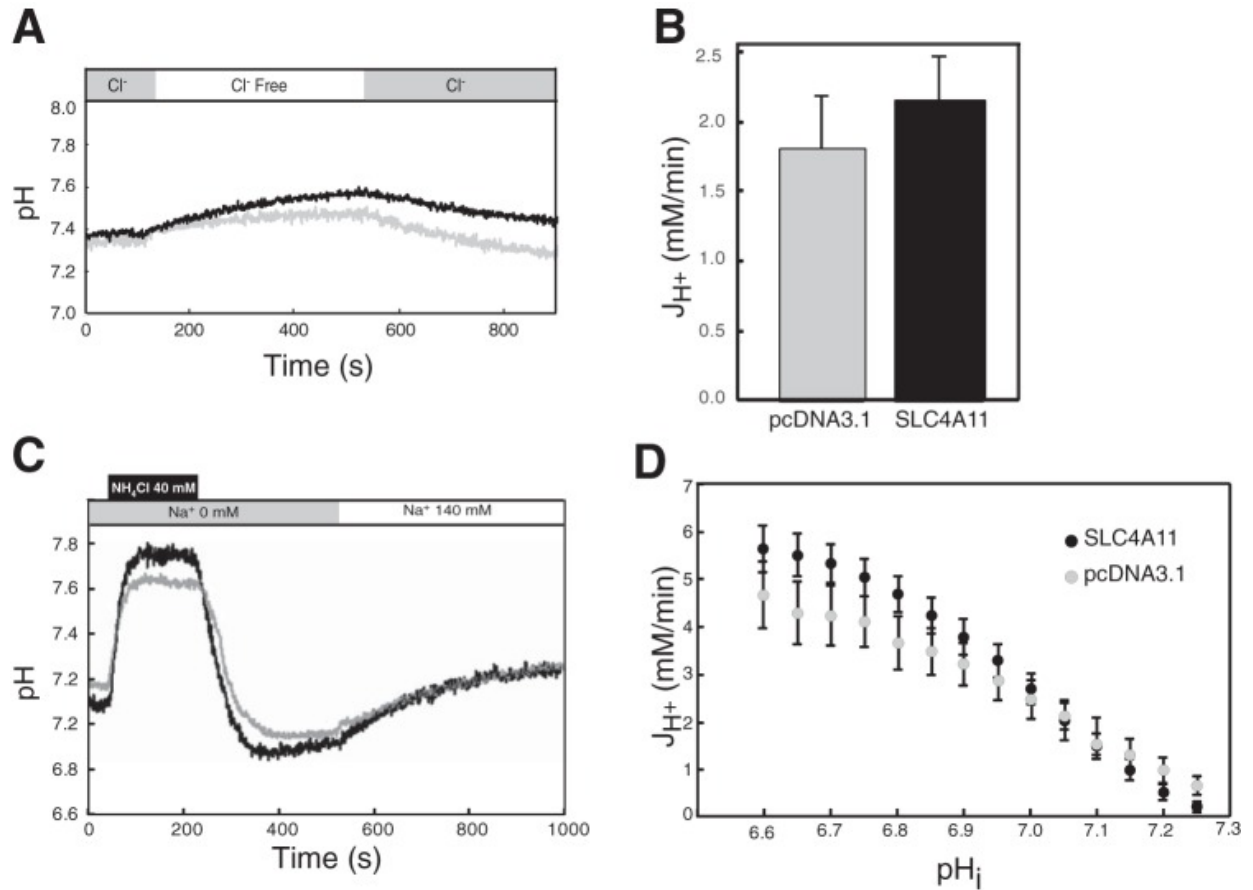
**Fig. 4.**



[Open in a separate window](#)

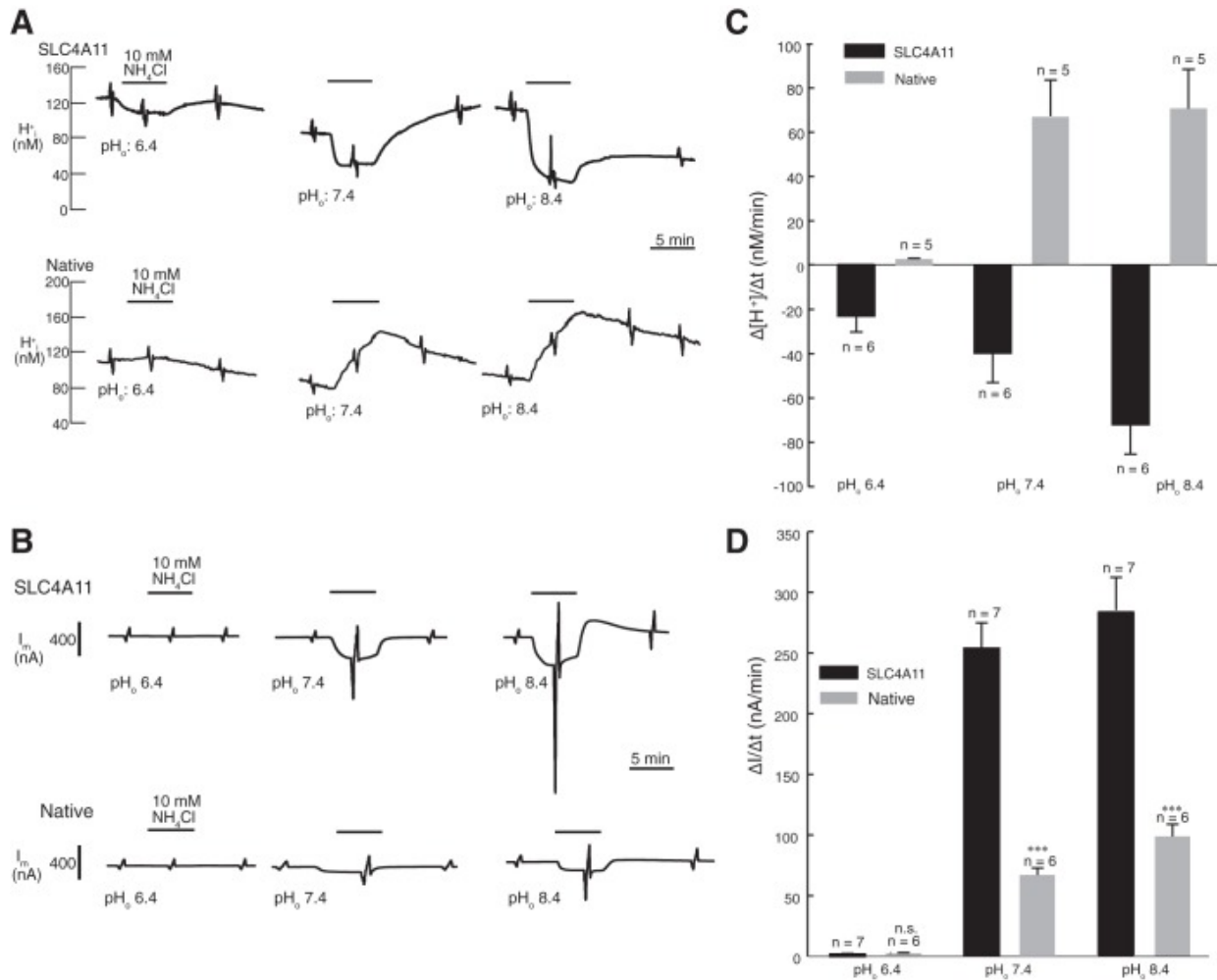
SLC4A11 does not exhibit current changes during Na<sup>+</sup> dependent or independent H<sup>+</sup>/OH<sup>-</sup>/HCO<sub>3</sub><sup>-</sup> changes in oocytes. SLC4A11 cRNA-injected or native oocytes were incubated for 72 h. pH and current were simultaneously measured with a double-barreled microelectrode combined with a two-electrode voltage clamp (clamped to -40 mV). *A* and *B*: current was measured when the native or SLC4A11-expressing oocytes, and were exposed to oocyte Ringer's solution (OR 7.4, white bar), OR containing only 10% Na<sup>+</sup>, adjusted to pH of 6.4 (10% Na<sup>+</sup> 6.4, black bar), OR containing bicarbonate (HCO<sub>3</sub><sup>-</sup> 7.4, gray bar), and OR containing only 10% Na<sup>+</sup> and HCO<sub>3</sub><sup>-</sup>, adjusted to pH of 6.4 (10% Na<sup>+</sup> HCO<sub>3</sub><sup>-</sup> 6.4, black bar). Arrows across the top bar indicate the time period when rates of [H<sup>+</sup>]<sub>i</sub> were measured, and the corresponding letters indicate the panel with the rates compared. *C*: membrane current mediated by SLC4A11 was calculated when oocytes were switched from OR 7.4 to 10% Na<sup>+</sup>, pH 6.4. *D* and *E*: membrane current mediated by SLC4A11 was calculated when oocytes were switched from OR 7.4 to HCO<sub>3</sub><sup>-</sup> 7.4 and then to 10% Na<sup>+</sup> and HCO<sub>3</sub><sup>-</sup>, pH 6.4. Error bars represent means ± SE (*n* = 7).

**Fig. 5.**



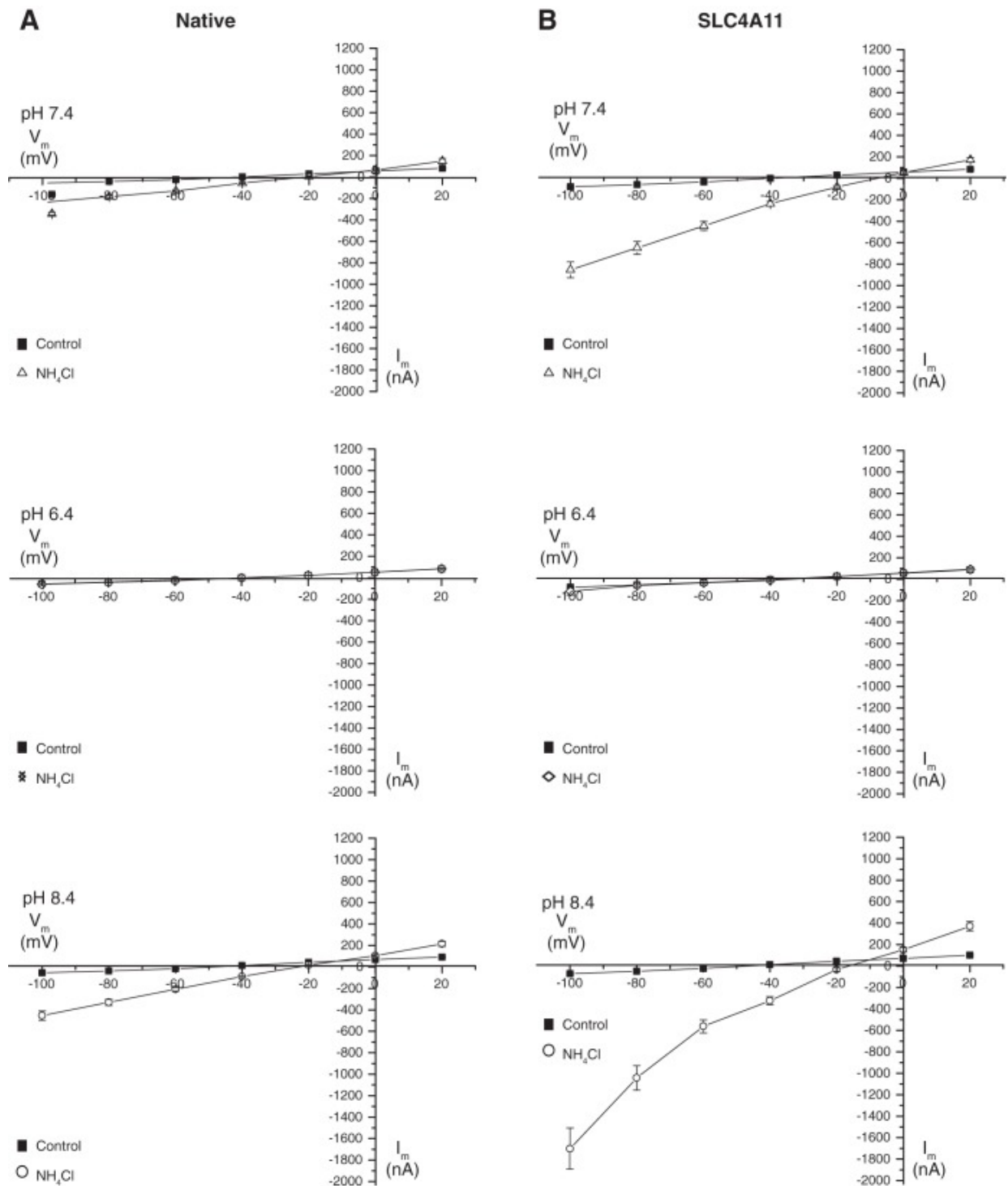
SLC4A11 does not transport bicarbonate. HEK293 cells, grown on glass coverslips and transfected with cDNA encoding SLC4A11 or empty vector, were incubated with the pH-sensitive dye BCECF-AM. Coverslips were placed in a fluorescence cuvette and fluorescence was monitored in a fluorimeter, using  $\lambda_{excitation} = 440$  and  $502.5$  nm and  $\lambda_{emission} = 528.7$  nm. *A*: cuvette was perfused alternately with Cl<sup>-</sup>-containing (shaded bar) and Cl<sup>-</sup>-free (open bar) Ringer's buffers, bubbled with 5% CO<sub>2</sub>. Black and gray traces represent results from cells transfected with SLC4A11 ( $n = 9$ ) and vector (pcDNA3.1,  $n = 7$ ), respectively. *B*: mean of Cl<sup>-</sup>/HCO<sub>3</sub><sup>-</sup> exchange activity ( $J_{H^+}$ ) calculated from the initial rate of pH<sub>i</sub> change during perfusion with Cl<sup>-</sup>-free buffer. *C*: sodium-dependent bicarbonate transport activity. BCECF-loaded HEK293 cells, transiently expressing SLC4A11 (black trace,  $n = 16$ ) or empty vector (gray trace  $n = 12$ ), were equilibrated in Na<sup>+</sup>-free Ringer's buffer (gray bar), containing  $5 \mu\text{M}$  ethyl-isopropyl amiloride (EIPA). All buffers in this experiment were bubbled with 5% CO<sub>2</sub>. NH<sub>4</sub>Cl was added (black bar) and then perfusion began with NH<sub>4</sub>Cl and Na<sup>+</sup>-free Ringer's buffer (gray bar). Finally, cuvette was perfused with Na<sup>+</sup>-containing Ringer's buffer (white bar). *D*: Na<sup>+</sup>-dependent bicarbonate transport activity estimated by [H<sup>+</sup>] flux ( $J_{H^+}$ ), following switching to Na<sup>+</sup>-containing medium (Student's *t*-test; all comparisons not significant for SLC4A11 vs. control at each tested pH value).

**Fig. 6.**



SLC4A11 mediates extracellular pH-dependent NH<sub>3</sub> permeability in oocytes. SLC4A11 cRNA-injected or native oocytes were incubated for 72 h. pH and current were simultaneously measured with a double-barreled microelectrode combined with a two-electrode voltage clamp (clamped to -40 mV). *A*: concentration of protons [H<sup>+</sup>]<sub>i</sub> was measured as the SLC4A11 (*top*) or native (*bottom*) expressing oocytes were exposed to oocyte Ringer's solution (OR) at pH 7.4, followed by OR containing 10 mM NH<sub>4</sub>Cl pH 7.4 (black bar), OR pH 6.4 followed by OR containing 10 mM NH<sub>4</sub>Cl pH 6.4, and OR pH 8.4 followed by OR containing 10 mM NH<sub>4</sub>Cl pH 8.4. Experiments were performed in the nominal absence of CO<sub>2</sub>/HCO<sub>3</sub><sup>-</sup>. *B*: current was measured when the native or SLC4A11-expressing oocytes were exposed to oocyte Ringer's solution (OR) at pH 7.4 followed by OR containing 10 mM NH<sub>4</sub>Cl pH 7.4 (black line), OR pH 6.4 followed by OR containing 10 mM NH<sub>4</sub>Cl pH 6.4, and OR pH 8.4 followed by OR containing 10 mM NH<sub>4</sub>Cl pH 8.4. *C*: rate of [H<sup>+</sup>]<sub>i</sub> change was calculated when oocytes were switched from OR to 10 mM NH<sub>4</sub>Cl at pH 7.4, 6.4, and 8.4. *D*: membrane current movement mediated by SLC4A11 was calculated when oocytes were switched from OR to OR containing 10 mM NH<sub>4</sub>Cl at pH 7.4, 6.4, and 8.4. Error bars represent means ± SE (*n* = 5–7). \*\*\*Significant difference (*P* ≤ 0.0001) compared with SLC4A11-expressing oocytes at same pH.

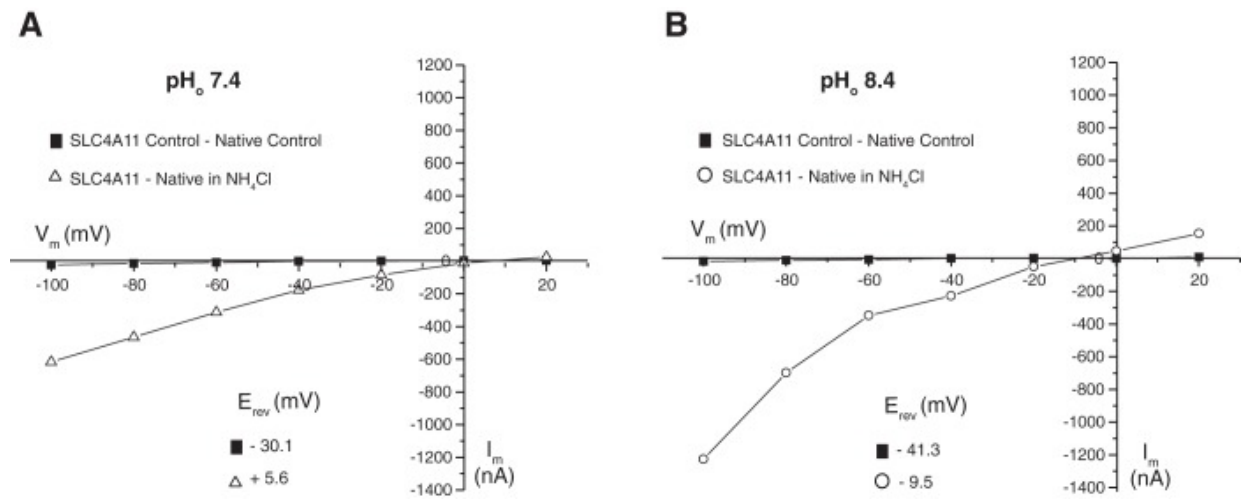
Fig. 7.



[Open in a separate window](#)

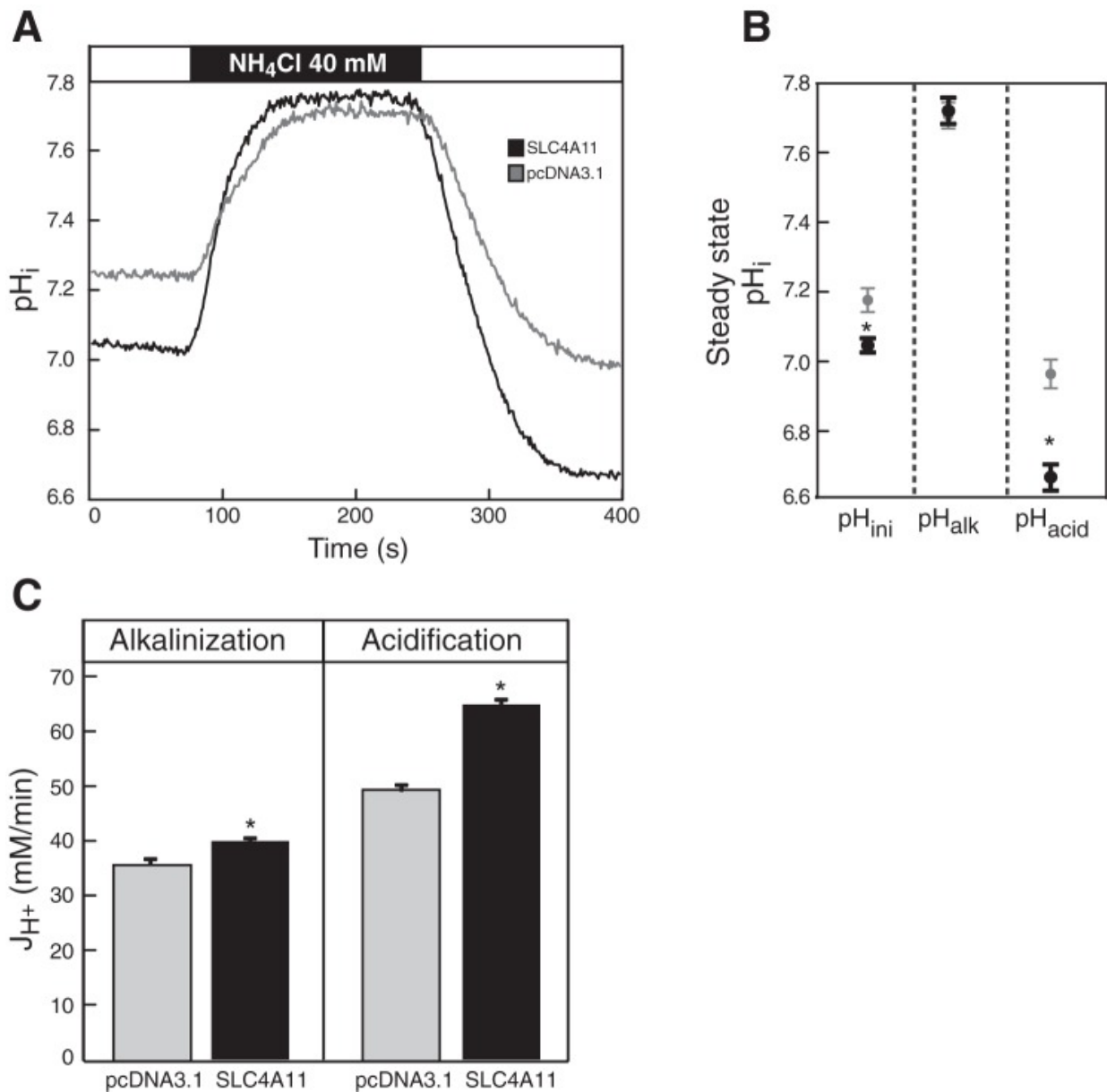
*I*-*V* relationships of native and SLC4A11-expressing oocytes in the presence of  $\text{NH}_4\text{Cl}$ . In native oocytes and SLC4A11-expressing oocytes, the current was recorded with a holding potential ( $V_h$ ) of  $-40$  mV, indicating the membrane conductance while perfused with Ringer's solution (control) and Ringer's solution containing  $10$  mM  $\text{NH}_4\text{Cl}$  at pH 7.4, 6.4, and 8.4. Experiments were performed in the nominal absence of  $\text{CO}_2/\text{HCO}_3^-$ . Current-voltage relationships of  $\text{NH}_4\text{Cl}$ -induced membrane currents, as obtained from experiments in Fig. 6, C and D, is shown for both for both native (A) and SLC4A11-expressing (B) oocytes. Error bars represent means  $\pm$  SE ( $n = 5-7$ ).

Fig. 8.



Net current-voltage ( $I-V$ ) relationships in the presence of  $\text{NH}_4\text{Cl}$ . Native oocytes and SLC4A11-expressing oocytes were voltage clamped to the indicated membrane potentials ( $V_m$ ), and current was monitored during perfusion with oocyte Ringer's buffer (control), or oocyte Ringer's buffer, containing 10 mM  $\text{NH}_4\text{Cl}$  at pH 7.4 ( $\text{NH}_4\text{Cl}$ ) (A) or pH 8.4 (B). Experiments were performed in the nominal absence of  $\text{CO}_2/\text{HCO}_3^-$ . Difference in current between SLC4A11-expressing and native oocytes was calculated in the absence (control) or presence ( $\text{NH}_4\text{Cl}$ ) of 10 mM  $\text{NH}_4\text{Cl}$ . Reversal potentials (inset,  $E_{rev}$ ) were calculated from the  $x$ -intercept values.

Fig. 9.



[Open in a separate window](#)

Ammonia transport facilitated by SLC4A11. HEK293 cells, grown on glass coverslips and transfected with cDNA encoding SLC4A11 ( $n = 16$ ) or empty vector (pcDNA3.1,  $n = 12$ ), were incubated with the pH-sensitive dye BCECF-AM. Coverslips were placed in a fluorescence cuvette, and fluorescence was monitored in a fluorimeter by using  $\lambda_{\text{excitation}} = 440$  and  $502.5$  nm and  $\lambda_{\text{emission}} = 528.7$  nm. Cuvette was perfused with Na<sup>+</sup>-free Ringer's buffer, containing 5  $\mu$ M ethyl-isopropyl amiloride (EIPA) (white bar), followed by the same buffer, containing 40 mM NH<sub>4</sub>Cl (black bar). *A*: representative traces of intracellular pH (pH<sub>i</sub>) changes. *B*: intracellular steady-state pH corresponding to the initial equilibrium in Ringer's buffer (pH<sub>ini</sub>), alkalization following NH<sub>4</sub>Cl perfusion (pH<sub>alk</sub>), and acidification following NH<sub>4</sub>Cl withdrawal (pH<sub>acid</sub>) states for pcDNA3.1-transfected (gray circles) and SLC4A11-expressing (black circles) cells. *C*: average [H<sup>+</sup>] flux ( $J_{\text{H}^+}$ ) during alkalization and acidification were calculated during the initial perfusion with NH<sub>4</sub>Cl-containing or following switch to NH<sub>4</sub>Cl-free buffer, respectively. Both groups were compared at the same pH for alkalization (pH = 7.30) and acidification (pH = 7.50) (Student's *t*-test, \* $P < 0.05$  for SLC4A11 vs. control).